2008

Analysis of shielded and open microstrip lines of double negative metamaterials using spectral domain approach (SDA)

Jianxing Ni
Iowa State University

Analysis of shielded and open microstrip lines of double negative metamaterials using

spectral domain approach (SDA)

by

Jianxing Ni

A thesis submitted to the graduate faculty

in partial fulfillment of the requirements for the degree of

MASTER OF SCIENCE

Major: Electrical Engineering

Program of Study Committee:
Jiming Song, Major Professor
Jaeyoun Kim
Rana Biswas

Iowa State University

Ames, Iowa

2008

TABLE OF CONTENTS

LIST OF FIGURES

LIST OF TABLES

ACKNOWLEDGEMENTS

I would like to take this opportunity to express my thanks to those who helped me with various aspects of conducting research and the writing of this thesis.

First of all, I would like to thank my major professor, Dr. Jiming Song, for his continuous support to my M.Sc. study. I thank him for his guidance, patience and support throughout this research and the writing of this thesis. His insights and motivation inspire me and guide me to complete the graduate education.

I would also like to thank my committee members: Dr. Rana Biswas, Dr. Jaeyoun Kim. Here, I thank you for your invaluable help, instruction, patience and time during the development of my work.

Of course, I sincerely thank my parents and uncle who always support me. I thank you for educating me during my life. Your love and words will be with me forever.

Finally my special thanks go to Tracy Wang. Thank you for standing by through the happy and frustration.

ABSTRACT

Double-negative (DNG) metamaterials, refer to artificially created materials both having negative permittivity and effective permeability at a given frequency. In the last several years, double negative metamaterials attract a great deal of attention from scientists.

In the area of high frequency application, transmission line serves as the fundamental building blocks. Due to the different application purposes, two kinds of microstrip are widely studied, shielded and open. In 2003, Krowne published his numerical results for shielded microstrip line with double negative metamaterials.

In this research, Chebyshev polynomials are chosen for the current basis functions and diverse model structures are analyzed. Spectral domain approach (SDA) is used to explore the electric guiding-wave properties of specific structures with DNG metamaterials, containing dispersion curves, field distributions, power flow, and characteristic impedance. Convergence test of the dispersion constant over different sizes of current basis is analyzed for the open microstrip. The numerical results show that propagating mode or complex mode is found at different frequencies and geometric setups. Field distributions show the significant difference from that of double positive (DPS) materials. To improve the calculation efficiency, numerical acceleration techniques are included and implemented. The numerical analysis implies that the shielding walls have great impact on the propagating properties in the shielded microstrip line. The open microstrip line filled with DNG metamaterials exhibits significant loss in its fundamental mode, indicating that it is not a good candidate for transmission line.

CHAPTER 1. OVERVIEW

1.1 Introduction

So far, the naturally-occurring materials exclusively obey the right-hand rule, which means that electric field $\vec{E}$, magnetic field $\vec{H}$, and wave vector $\vec{k}$ are in the right hand rule. In the view of media parameters, the right hand rule implies that the permittivity and permeability are both positive. So the conventional materials are usually called right-hand materials (RHM) or double positive (DPS) materials. While, double negative (DNG) metamaterials are artificially patterned metal-dielectric structures. Due to the negative permittivity and permeability, the electric field, magnetic field and wave vector follow the left hand rule instead of right hand rule. So DNG metamaterials are also called left-hand metamaterials (LHM). In DNG metamaterials, the group velocity and phase velocity are in different directions. Thus, the direction of phase velocity is opposite to that of the energy velocity. This interesting property will cause the negative-index of refraction. So DNG metamaterials are also called negative index metamaterials (NIM).

DNG metamaterials were first proposed by a Russian scientist Veselago in 1968 [1]. The new properties of DNG metamaterials were analyzed, such as negative index of refraction, opposite group and phase velocity, reversed Doppler effect [1, 2, 3].

After Veselago's work, only much later, LHM began to attract the attention of scientist. In the last several years, DNG metamaterials attract a great deal of attention from scientist and researchers. In 1999, Pendry and his colleagues analyzed a metamaterial, which had negative

permeability. Pendry also published on subjects such as surface plasmas and negative refractive index materials [4, 5].

In 2000, D. R. Smith and his colleagues made impressive progress in the field of DNG metamaterials. They fabricated a periodical structure that simultaneously had negative permeability and negative permittivity in a small frequency range [6]. One year later, in the experiments, they observed negative refraction index [7, 8]. All these pioneer works give birth to a new field of research (DNG metamaterials). After that, a great deal of attentions from scientific and engineering communities is paid to the DNG metamaterials.

In 2003, Krowne published his numerical results of the shielded microstrip line with DNG metamaterials [22]. In W. Shu's Ph.D thesis, dielectric slab with DNG metamaterials is analyzed. The dispersion properties for the DNG dielectric slab are obtained [16]. He also worked on the open microstrip line with DNG metamaterials and got the dispersion curves [17].

In this thesis, spectrum domain approach (SDA), which is a full-wave method that solves the Maxwell's equation directly to find appropriate solutions that satisfy some boundary conditions, is used to explore the electromagnetic guiding-wave properties of specific structures with double negative metamaterials, containing dispersion curves, field distribution, power flow, and characteristic impedance. Two microstrip models, which are shielded and open, are analyzed. Chebyshev polynomials with coefficients are used to expand the unknown current distribution. For both of shielded and open microstrip lines, propagating mode or complex mode is found at different frequencies and geometric setups. The field distributions in spatial domain show the significant difference from that of double positive materials. To reduce the calculation cost, numerical acceleration techniques, such as leading

term extraction, are included and implemented. Numerical results imply that the shielding walls have great impact on the propagating properties in the shielded microstrip line. The open microstrip line with DNG metamaterials possesses significant loss in its fundamental mode, which indicates that it is not a good candidate for a transmission line.

1.2 Research motivation

As the developing of communication industry, the high frequency circuit design begins to be more critical. The planar passive transmission line is extensively implemented in modern high frequency circuits. In the industry, most of interconnections and passive networks are consisted of transmission lines. For example, the matching networks in power amplifier can be realized by the transmission stubs. The de-embedding techniques for the MMIC (Monolithic Microwave Integrated Circuits) components require SOLT (short-open-load-through) transmission structures to shift the phase reference plane to the DUT (device under test). In receiver design, the filter can be implemented by transmission stubs or couple lines.

For the transmission line, the properties are directly relevant to its medium parameters. For example, the phase velocity of a transmission line mainly depends on its dielectric constant, especially the real part.

As the operating frequency increases, the parasitic effects in microstrip line begin to be significant. For example, in GaAs based MMIC, the Q (quality factor) of printed inductor is very low due to the thin dielectric, which can increase the parasitic capacitor. Therefore, it is meaningfully and worthwhile to investigate the properties of transmission lines with DNG metamaterials.

According to the different application fields, the transmission lines can be modeled as open or shielded. Figure 1.1 shows two microstrip lines with DNG metamaterials that will be solved in this thesis.

(a) Open microstrip line   (b) Shielded microstrip line
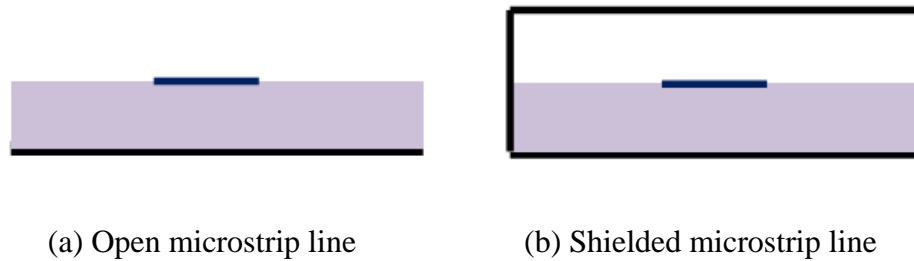
Figure 1.1 Open and shielded microstrip Lines with DNG metamaterisls below the strip and air above.

With these motivations, we move to the numerical analysis of the DNG metamaterials. To predict accurately the electrical performance of the transmission lines over a given frequency band, the full-wave spectral domain approach is applied [9, 10, 11]. In order to simplify the problem, Fourier transform is performed over x direction. In spectral domain, the boundary conditions are used to derive the Green's functions. Chebyshev polynomials are chosen for the current basis functions. Then method of moments is applied to get the dispersion properties. With the obtained propagation constant, the spatial domain field can be calculated from the spectral domain fields by inverse Fourier transform. With the Parseval's theorem, the total power can be calculated.

1.3 Organization of the thesis

The rest part of the thesis is organized as follows. Chapter 2 investigates the shielded microstrip lines. Spectral domain analysis is applied to get the potential, field, Green's

functions etc. Current basis functions of Chebyshev polynomials are also included. Then method of moments is applied to get the dispersion properties. At a given frequency, the propagation constant can be solved. Then the field distributions in spatial domain, total power, and characteristic impedance are derived.

Chapter 3 provides the numerical considerations and results. First, in order to reduce the CPU time of the calculation, some numerical acceleration techniques are analyzed and implemented. Then the numerical results such as dispersion curves, field distribution, power flow, and characteristic impedance are provided. The summary and future works go to Chapter 4.

In Appendix A, the spectral analysis of open microstrip lines with DNG metamaterials is provided, which is similar to the shielded case.

CHAPTER 2. SHIELDED MICROSTRIP LINE WITH DNG METAMATERIALS

In modern microwave/RF systems and circuits, transmission line is widely used. Among the transmission lines, microstrip is the one that mostly used. Studying the properties of microstrip line with DNG metamaterials will provide us a fundamental understanding of the DNG metamaterisl. In the following chapters, several microstrip models, containing shielded microstrip, open microstrop, will be analyzed. The spectral domain approach is applied to get the dispersion properties, based on which we will get other information, such as field distribution, power, impedance [9, 10, 11].

2.1 Introduction

In the last several years, a lot of theoretical simulation and analysis have been conducted, concerning the properties of DNG material. In current high frequency circuit design, the transmission line such as: microstrip line, strip line, CPW line with double positive material are clearly understood and widely used by the modern RF/Microwave engineers [12]. While, when moving to the DNG material, we find that there are many interesting and attractive features, such as the dispersion curves with complex mode, different field distribution from the microstrip with DPS materials.

2.1.1 Model setup

In the application, multilayer-microstrip is often considered for compact layout and cost saving. It is meaningful to study the microstrip with perfect electric conductor (PEC)

walls for shielding. In this chapter, we will study the properties of the shielded microstrip lines with DNG materials. Spectral domain approach is utilized for numerical calculations.
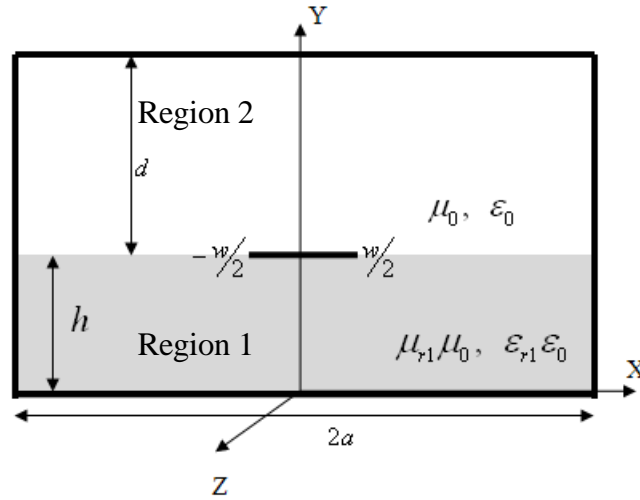
Figure 2.1 Shielded microstrip line

Figure 2.1 shows the cross section view of the shielded microstrip line. In this model, the DNG metamaterial is layered on the bottom PEC wall with a thickness of h. Above the DNG metamaterial, it is filled with air. At the interface of the two dielectrics, an infinite thin strip is placed with a width of w. Moreover, there is a top layer of perfect conductor placed with a height of d above the strip. Two side walls of PEC are placed symmetrically with $2a$ distance.

2.2 Spectral domain analysis

Due to the phase matching at the interface of air and DNG metamaterial, pure TEM (transverse electromagnetic) mode cannot be supported in this microstrip model. So in spectral domain approach, we use the hybrid modes instead of pure TEM mode, then a superposition of

infinite TEz (transverse electric) and TMz (transverse magnetic) modes can be analyzed [13]. Vector potentials can be used to express all the field components.

2.2.1 **Vector potential**

In the analysis of electromagnetic problems with boundary conditions, it is common practice to use auxiliary vector potentials to get the solutions. The most used are magnetic vector potential ($\vec{A}$) and electrical vector potential ($\vec{F}$).

For TMz mode, the vector potential is given as:

$$A_{zi}(x, y, z) = -\frac{\omega \mu_i \varepsilon_i}{\beta} \Phi_i^{(e)}(x, y) e^{-j\beta z} \tag{2.1}$$

For TEz mode:

$$F_{zi}(x, y, z) = -\frac{\omega \mu_i \varepsilon_i}{\beta} \Phi_i^{(h)}(x, y) e^{-j\beta z} \tag{2.2}$$

The scale potentials satisfy the Helmholtz equations at $y \neq h$:

$$\nabla_t^2 \Phi_i^{(p)}(x, y) + \left(k_i^2 - \beta^2\right) \Phi_i^{(p)}(x, y) = 0 \tag{2.3}$$

in which, $k_i^2 = \omega^2 \varepsilon_i \mu_i$, $i = 1, 2$, $p = e, h$.

Solving the Helmholtz equations, all of the field components are derived

$$E_{xi}(x, y) = \frac{\partial \Phi_i^{(e)}}{\partial x} + \frac{\omega \mu_i}{\beta} \frac{\partial \Phi_i^{(h)}}{\partial y}$$

$$E_{yi}(x, y) = \frac{\partial \Phi_i^{(e)}}{\partial y} - \frac{\omega \mu_i}{\beta} \frac{\partial \Phi_i^{(h)}}{\partial x}$$

$$E_{zi}(x, y) = j \frac{k_i^2 - \beta^2}{\beta} \Phi_i^{(e)}$$

$$H_{xi}(x, y) = \frac{\partial \Phi_i^{(h)}}{\partial x} - \frac{\omega \varepsilon_i}{\beta} \frac{\partial \Phi_i^{(e)}}{\partial y}$$

$$H_{yi}(x, y) = \frac{\partial \Phi_i^{(h)}}{\partial y} + \frac{\omega \varepsilon_i}{\beta} \frac{\partial \Phi_i^{(e)}}{\partial x}$$

$$H_{zi}(x, y) = j \frac{k_i^2 - \beta^2}{\beta} \Phi_i^{(h)} \qquad (2.4)$$

In the above field expression, one should notice that $e^{-j\beta z}$ is dropped.

2.2.2 Fourier series

In spectral domain analysis, we apply Fourier transform over x to reduce the partial differential equations (PDE) to ordinary differential equations (ODE).

Due to the shielded side walls, the vector potentials are only defined for x from $-a$ to a. So in shielded microstrip line, the inverse Fourier transform should be changed to series summation.

$$\tilde{\Phi}_i^{(p)}(n, y) = \int_{-a}^{a} dx \Phi_i^{(p)}(x, y) e^{j\alpha_n x} \qquad (2.5)$$

$$\Phi_i^{(p)}(x, y) = \frac{1}{2a} \sum_{m=-\infty}^{\infty} \tilde{\Phi}_i^{(p)}(m, y) e^{-j\alpha_m x} \qquad (2.6)$$

in which, $i = 1, 2$, $p = e, h$, $\alpha_m = m\pi/a$.

In (2.6), a full range summation is included. To reduce the CPU time, we applied boundary conditions on the field component.

Considering the field components in (2.4), the electric field components E_z and E_y, for the fundamental quasi-TEM mode, should be an even function of x, so

$$\begin{aligned} \Phi_i^{(e)}(x, y) &\sim \cos(\alpha_m x) \\ \Phi_i^{(h)}(x, y) &\sim \sin(\alpha_m x) \end{aligned} \qquad (2.7)$$

On two side walls, the tangential electrical fields meet the PEC boundary condition, so

$$E_z\big|_{x=\pm a} = E_y\big|_{x=\pm a} = 0 \Rightarrow \begin{cases} \Phi_i^{(e)}(a, y) = 0 \\ \Phi_i'^{(h)}(a, y) = 0 \end{cases} \qquad (2.8)$$

Substitute the potential into the field expressions, then we arrive at

$$\cos\left(\alpha_m x\right) = 0 \Rightarrow \begin{cases} \alpha_m a = m\pi/2 \\ m = 2n-1 \end{cases} \tag{2.9}$$

so m is odd. (2.7) implies that $\Phi_i^{(e)}\left(x, y\right)$ is an even function of x, and $\Phi_i^{(h)}\left(x, y\right)$ is an odd function of x.

Rewriting (2.9), we get

$$\alpha_n = \left(n-1/2\right)\pi/a \tag{2.10}$$

Now, let's return to the Fourier transform. In the shielded microstrip line, all of the fields components and potentials are defined for x from $-a$ to a. If we expand the expressions as periodic functions of x with a period of $4a$. Then we can get

$$\tilde{f}\left(m\right) = \int_{-2a}^{2a} dx f\left(x\right) e^{j\alpha_m x} \tag{2.11}$$

$$f\left(x\right) = \frac{1}{4a} \sum_{m=-\infty}^{\infty} \tilde{f}\left(m\right) e^{-j\alpha_m x} \tag{2.12}$$

If $f\left(x\right)$ is an even function, (2.11) can be rewritten as

$$\begin{aligned} \tilde{f}\left(m\right) &= 2\int_0^{2a} dx f\left(x\right)\cos\left(\alpha_m x\right) \\ &= 2\int_0^{a} dx f\left(x\right)\cos\left(\alpha_m x\right) + 2\int_a^{2a} dx f\left(x\right)\cos\left(\alpha_m x\right) \end{aligned} \tag{2.13}$$

let $x = 2a - x'$

$$\int_a^{2a} dx f\left(x\right)\cos\left(\alpha_m x\right) = -\int_0^{a} dx' f\left(2a - x'\right)\cos\left[m\pi x'/(2a)\right] \tag{2.14}$$

Combining the two parts together, it comes to

$$\tilde{f}\left(m\right) = 2\int_0^{a} dx\left[f\left(x\right) - f\left(2a - x\right)\right]\cos\left(\alpha_m x\right) \tag{2.15}$$

Therefore, if we expand the $f\left(x\right)$ as

$$f(x) = -f(2a-x) \qquad a < x < 2a \tag{2.16}$$

With $f(a) = 0$, we get

$$\tilde{f}(n) = 4\int_0^a dx f(x)\cos(\alpha_n x) = 2\int_{-a}^a dx f(x)e^{j\alpha_n x} \tag{2.17}$$

$$f(x) = \frac{1}{2a}\sum_{n=1}^{\infty} \tilde{f}(n)\cos(\alpha_n x) \tag{2.18}$$

Similarly, if $f(x)$ is an odd function and $f'(a) = 0$, we expand as

$$f(x) = f(2a-x) \qquad a < x < 2a \tag{2.19}$$

$$\tilde{f}(n) = 4j\int_0^a dx f(x)\sin(\alpha_n x) = 2\int_{-a}^a dx f(x)e^{j\alpha_n x} \tag{2.20}$$

$$f(x) = \frac{-j}{2a}\sum_{n=1}^{\infty} \tilde{f}(n)\sin(\alpha_n x) \tag{2.21}$$

(2.18) and (2.21) implies that the modified inverse Fourier series can cut the summation time

to half. It will improve the numerical efficiency.

As illustrated above, $\Phi_i^{(e)}(x,y)$ is even and $\Phi_i^{(h)}(x,y)$ is odd. Applying to (2.18) and

(2.21) on them, we get the spatial scale potentials.

$$\Phi_i^{(p)}(x,y) = \frac{1}{2a}\sum_{m=-\infty}^{\infty} \Phi_i^{(p)}(m,y)e^{j\alpha_m x} = \frac{1}{a}\left\{ \begin{array}{l} \displaystyle\sum_{n=1}^{\infty} \Phi_i^{(e)}(n,y)\cos(\alpha_n x) \\ \displaystyle -j\sum_{n=1}^{\infty} \Phi_i^{(h)}(n,y)\sin(\alpha_n x) \end{array} \right. \tag{2.22}$$

where $\alpha_n = (n-1/2)\pi/a$

To reduce the partial differential equation (PDE) in (2.3) to ordinary differential

equation (ODE), we conduct Fourier transform on the two sides of (2.3). Then the Helmholtz

equations in spectral domain is

$$\left(\frac{d^2}{dy^2} - \gamma_i^2\right)\tilde{\Phi}_i^{(p)}(\alpha, y) = 0 \tag{2.23}$$

(2.23) is an ordinary differential equation, there are two kinds of general solutions depending on the boundary conditions.

$$\tilde{\Phi}_i^{(p)}(n, y) = A_i^{(p)}(n)e^{\gamma_i y} + B_i^{(p)}(n)e^{-\gamma_i y} \tag{2.24}$$

or $$\tilde{\Phi}_i^{(p)}(n, y) = C_i^{(p)}(n)\sinh(\gamma_i y) + D_i^{(p)}(n)\cosh(\gamma_i y) \tag{2.25}$$

In spectral domain, the field components in (2.4) are y and α dependant.

$$
\begin{aligned}
\tilde{E}_{xi}(\alpha, y) &= (-j\alpha)\tilde{\Phi}_i^{(e)}(\alpha, y) + \frac{\omega\mu_i}{\beta}\frac{\partial}{\partial y}\tilde{\Phi}_i^{(h)}(\alpha, y) \\
\tilde{E}_{yi}(\alpha, y) &= \frac{\partial}{\partial y}\tilde{\Phi}_i^{(e)}(\alpha, y) + j\alpha\frac{\omega\mu_i}{\beta}\tilde{\Phi}_i^{(h)}(\alpha, y) \\
\tilde{E}_{zi}(\alpha, y) &= j\frac{k_i^2 - \beta^2}{\beta}\tilde{\Phi}_i^{(e)}(\alpha, y) \\
\tilde{H}_{xi}(\alpha, y) &= (-j\alpha)\tilde{\Phi}_i^{(h)}(\alpha, y) - \frac{\omega\varepsilon_i}{\beta}\frac{\partial}{\partial y}\tilde{\Phi}_i^{(e)}(\alpha, y) \\
\tilde{H}_{yi}(\alpha, y) &= \frac{\partial}{\partial y}\tilde{\Phi}_i^{(h)}(\alpha, y) + (-j\alpha)\frac{\omega\varepsilon_i}{\beta}\tilde{\Phi}_i^{(e)}(\alpha, y) \\
\tilde{H}_{zi}(\alpha, y) &= j\frac{k_i^2 - \beta^2}{\beta}\tilde{\Phi}_i^{(h)}(\alpha, y)
\end{aligned}
\tag{2.26}
$$

Correspondingly, $e^{-j\beta z}$ is also dropped.

2.2.3 Boundary conditions

In the previous parts, we derive the solutions to Helmholtz equations in spectral domain and get two kinds of general solutions, which depend on the different boundary conditions.

For PEC layer at the bottom and top, the boundary conditions are that the tangential components of electric field are zero, so

$$\tilde{E}_{z1}(n,0) = \tilde{E}_{z2}(n,h+d) = 0 \Rightarrow \tilde{\Phi}_1^{(e)}(n,0) = \tilde{\Phi}_2^{(e)}(n,h+d) = 0 \tag{2.27}$$

$$\tilde{E}_{x1}(n,0) = \tilde{E}_{x2}(n,h+d) = 0 \Rightarrow \frac{\partial}{\partial y}\Phi_1^{(h)}(n,0) = 0 = \frac{\partial}{\partial y}\tilde{\Phi}_2^{(h)}(n,n+h) = 0 \tag{2.28}$$

With (2.27), (2.28), and (2.24) can be reduced to

$$\tilde{\Phi}_1^{(e)}(n,y) = A(n)\sinh(\gamma_1 y) \tag{2.29}$$

$$\tilde{\Phi}_1^{(h)}(n,y) = C(n)\cosh(\gamma_1 y) \tag{2.30}$$

$$\tilde{\Phi}_2^{(e)}(n,y) = B(n)\frac{\sinh\left[\gamma_2(h+d-y)\right]}{\sinh(\gamma_2 d)} \tag{2.31}$$

$$\tilde{\Phi}_2^{(h)}(n,y) = D(n)\frac{\cosh\left[\gamma_2(h+d-y)\right]}{\cosh(\gamma_2 d)} \tag{2.32}$$

(2.26) implies that, to get the field components, the potentials expansion coefficients are demanded. While, there is one unknown in each potential expression. So at least, we need four more equations to solve them.

The tangential electrical fields of two regions at the interface are continuous. So in spectral domain:

$$\begin{aligned} \tilde{E}_{z1}(n,h) &= \tilde{E}_{z2}(n,h) \\ \tilde{E}_{x1}(n,h) &= \tilde{E}_{x2}(n,h) \end{aligned} \tag{2.33}$$

Substitute the field components into (2.33), we arrive at

$$\begin{aligned} \left(k_1^2 - \beta^2\right)A\sinh(\gamma_1 h) &= \left(k_2^2 - \beta^2\right)B \\ j\alpha_n\left[A\sinh(\gamma_1 h) - B\right] &= \frac{\omega}{\beta}\left[\gamma_1\mu_1 C\sinh(\gamma_1 h) + \gamma_2\mu_2 D\tanh(\gamma_2 d)\right] \end{aligned} \tag{2.34}$$

For infinite thin strip, no current component flows in y-direction. So surface electric current is considered in x-and z-direction, which is denoted as

$$\vec{J}_s(x,z) = \left[\hat{x}J_x(x) + \hat{z}J_z(x)\right]e^{-j\beta z} \tag{2.35}$$

Then the magnetic field boundary conditions in spatial domain yield

$$\hat{y} \times \left(\vec{H}_2 - \vec{H}_1\right) = \vec{J}_s \tag{2.36}$$

In spectral domain, the boundary conditions can be written as

$$\begin{aligned} H_{z2}(n,h) - H_{z1}(n,h) &= \tilde{J}_x(n) \\ H_{x2}(n,h) - H_{x1}(n,h) &= -\tilde{J}_z(n) \end{aligned} \tag{2.37}$$

Substitute the vector expression into the above equations and rewrite the two equations:

$$\begin{aligned} \left(k_1^2 - \beta^2\right)\cosh(\gamma_1 h)C - \left(k_2^2 - \beta^2\right)D &= j\beta\tilde{J}_x(n) \\ j\omega\varepsilon_1\gamma_1\cosh(\gamma_1 h)A + j\omega\varepsilon_2\gamma_2\coth(\gamma_2 d)B - \alpha_n\beta\cosh(\gamma_1 h)C + \alpha_n\beta D &= -j\beta\tilde{J}_z \end{aligned} \tag{2.38}$$

So far, we have four equations with four unknowns, we can solve them to get the solutions. To simplify the problem solving, all of the elements are filled into a matrix as:

$$\begin{pmatrix} -P_1^2\sinh(\gamma_1 h) & P_2^2 & 0 & 0 \\ \alpha_n\beta\sinh(\gamma_1 h) & -\alpha_n\beta & j\omega\gamma_1\mu_1\sinh(\gamma_1 h) & j\omega\gamma_2\mu_2\tanh(\gamma_2 d) \\ 0 & 0 & P_1^2\cosh(\gamma_1 h) & -P_2^2 \\ j\omega\varepsilon_1\gamma_1\cosh(\gamma_1 h) & j\omega\varepsilon_2\gamma_2\coth(\gamma_2 d) & -\alpha_n\beta\cosh(\gamma_1 h) & \alpha_n\beta \end{pmatrix}\begin{pmatrix} A \\ B \\ C \\ D \end{pmatrix} = \begin{pmatrix} 0 \\ 0 \\ j\beta\tilde{J}_x \\ -j\beta\tilde{J}_z \end{pmatrix} \tag{2.39}$$

in which, $P_1^2 = k_1^2 - \beta^2$, $P_2^2 = k_2^2 - \beta^2$.

According to (2.34) and (2.38), we can derive the following relations:

$$\begin{aligned} A &= \frac{P_2^2 B}{P_1^2\sinh(\gamma_1 h)} \\ C &= \frac{P_2^2 D}{P_1^2\cosh(\gamma_1 h)} + \frac{j\beta\tilde{J}_x}{P_1^2\cosh(\gamma_1 h)} \end{aligned} \tag{2.40}$$

Substituting A and C into the matrix, comes to

$$\begin{pmatrix} B \\ D \end{pmatrix} = \frac{1}{\Delta}\begin{pmatrix} -b_{22} & -b_{12} \\ -b_{21} & -b_{11} \end{pmatrix}\begin{pmatrix} F_1\tilde{J}_x \\ \dfrac{\alpha\beta}{P_1^2}\tilde{J}_x - \tilde{J}_z \end{pmatrix} \tag{2.41}$$

where

$$b_{11} = -b_{22} = \frac{j\alpha_n}{k_1^2 - \beta^2}\left(k_2^2 - k_1^2\right)$$

$$b_{12} = \frac{\omega}{\beta\left(k_1^2 - \beta^2\right)}\left[\gamma_2\mu_2\left(k_1^2 - \beta^2\right)\tanh\left(\gamma_2 d\right) + \gamma_1\mu_1\left(k_2^2 - \beta^2\right)\tanh\left(\gamma_1 h\right)\right]$$

$$b_{21} = \frac{\omega}{\beta\left(k_1^2 - \beta^2\right)}\left[\gamma_2\varepsilon_2\left(k_1^2 - \beta^2\right)\coth\left(\gamma_2 d\right) + \gamma_1\varepsilon_1\left(k_2^2 - \beta^2\right)\coth\left(\gamma_1 h\right)\right]$$

$$F_1 = \frac{\omega\mu_1\gamma_1\tanh\left(\gamma_1 h\right)}{j\left(k_1^2 - \beta^2\right)}$$

$$\tag{2.42}$$

$$\Delta = \left[\mu_2\gamma_1\coth\left(\gamma_1 h\right) + \mu_1\gamma_2\coth\left(\gamma_2 d\right)\right]\left[\varepsilon_2\gamma_1\tanh\left(\gamma_1 h\right) + \varepsilon_1\gamma_2\tanh\left(\gamma_2 d\right)\right]$$

$$\tag{2.43}$$

To this end, the ABCD parameters are derived [9]. However, we still have many unknowns, such as the surface current, propagating constant etc.

2.2.4 Green functions

In order to know the guiding properties of the shielded microstrip, the propagating constant needs to be solved. Thus, more coupled equations are demanded. With the parameters from boundary conditions, now we can derive the expressions for the Green functions.

First we rewrite the field of the spectrum domain at the interface as the form of vector potential

$$\tilde{E}_{x2}\left(n,h\right) = -j\alpha_n\tilde{\Phi}_2^{(e)}\left(n,h\right) + \frac{\omega\mu_2}{\beta}\gamma_2\frac{\partial}{\partial y}\tilde{\Phi}_2^{(h)}\left(n,h\right)$$

$$= -j\alpha_n B\left(n\right) - \frac{\omega\mu_2}{\beta}\gamma_2\tanh\left(\gamma_2 d\right)D\left(n\right)$$

$$\tag{2.44}$$

$$\tilde{E}_{z2}\left(n,h\right) = j\frac{k_2^2 - \beta^2}{\beta}\tilde{\Phi}_2^{(e)}\left(n,h\right) = j\frac{k_2^2 - \beta^2}{\beta}B\left(n\right)$$

$$\tag{2.45}$$

Then we can change the forms of the fields to Green's functions

$$\tilde{E}_{x2}(n,h) = G_{xx}(n,\beta)\tilde{J}_x(n) + G_{xz}(n,\beta)\tilde{J}_z(n)$$
$$\tilde{E}_{z2}(n,h) = G_{zx}(n,\beta)\tilde{J}_x(n) + G_{zz}(n,\beta)\tilde{J}_z(n)$$
(2.46)

where

$$G_{xx}(n,\beta) = \frac{-j\eta_2}{k_2\Delta}\Big[\big(k_1^2 - \alpha_n^2\big)\gamma_2\tanh(\gamma_2 d) + \mu_r\big(k_2^2 - \alpha_n^2\big)\gamma_1\tanh(\gamma_1 h)\Big]$$

$$G_{xz}(n,\beta) = G_{zx}(n,\beta) = \frac{-j\eta_2\alpha_n\beta}{k_2\Delta}\big[\gamma_2\tanh(\gamma_2 d) + \mu_r\gamma_1\tanh(\gamma_1 h)\big]$$
(2.47)

$$G_{zz}(n,\beta) = \frac{-j\eta_2}{k_2\Delta}\Big[\big(k_1^2 - \beta^2\big)\gamma_2\tanh(\gamma_2 d) + \mu_r\big(k_2^2 - \beta^2\big)\gamma_1\tanh(\gamma_1 h)\Big]$$

$$\Delta = \Big[\varepsilon_r\gamma_2\tanh(\gamma_2 d) + \gamma_1\tanh(\gamma_1 h)\Big]\Big[\mu_r\gamma_2\coth(\gamma_2 d) + \gamma_1\coth(\gamma_1 h)\Big]$$

in which, $\varepsilon_r = \varepsilon_1/\varepsilon_2$, $\mu_r = \mu_1/\mu_2$

2.3 Method of moments

2.3.1 Current basis functions

So far, we still do not know the current distribution on the strip. But the current can be expanded with basis functions with unknown coefficients. Moreover, the basis functions must be chosen such that their inverse Fourier transforms are nonzero only on the strip $|x| \le w/2$.

In this thesis, the transverse current and longitudinal current are approximated by the expansions of Chebyshev polynomials with singularity [13, 14].

$$J_x(x) = j\sqrt{1 - (2x/w)^2}\sum_{n=1}^{M} I_{xn}U_{2n-1}(2x/w)$$
$$J_z(x) = \frac{1}{\sqrt{1 - (2x/w)^2}}\sum_{n=1}^{N} I_{zn}T_{2n-2}(2x/w)$$
(2.48)

where $T_n(x)$ and $U_n(x)$ are the first kind and second kind of Chebyshev polynomials.

Applying Fourier transform to the above current basis, we come to:

$$\tilde{J}_x(m) = \sum_{n=1}^{M} a_n J_{2n}(\delta_m)/\alpha_m$$

$$\tilde{J}_z(m) = \sum_{n=1}^{N} b_n J_{2(n-1)}(\delta_m)$$

(2.49)

where $a_n = (-1)^n 2\pi n I_{xn} w$, $b_n = (-1)^{n-1} \pi I_{zn} w/2$, $\delta_m = \alpha_m w/2$, $J_n(x)$ is the Bessel function of the first kind.

2.3.2 Galerkin's methods

For the shielded microstrip line, the tangential components of electrical field at the interface of region 1 and region 2 are given in (2.46). The current expansion parameters and the fields out of strip in spectral domain are unknowns. For the above coupled equations, Galerkin's method can be applied in the Fourier transform domain.

The Parseval's theorem is:

$$\sum_{-\infty}^{\infty} \tilde{f}(n)\tilde{g}(n) = \frac{1}{2a}\int_{-a}^{a} dx f(x)g(-x)$$

(2.50)

At the height of h, the field satisfies the conditions:

$$E_{z1}(x,h) = E_{z2}(x,h) = \begin{cases} 0 & |x| < w/2 \\ \text{unkown} & |x| > w/2 \end{cases}$$

(2.51)

$$E_{x1}(x,h) = E_{x2}(x,h) = \begin{cases} 0 & |x| < w/2 \\ \text{unkown} & |x| > w/2 \end{cases}$$

(2.52)

While the current satisfies the following conditions:

$$J_x(x), J_z(x) = \begin{cases} \text{unknown} & |x| < w/2 \\ 0 & |x| > w/2 \end{cases}$$

(2.53)

We have four unknowns here. In order to simplify the calculation, we write their products in the whole x range as:

$$E_{qi}(x)J_q(-x) = 0 \tag{2.54}$$

where $q = x, z, \; i = 1, 2$

Applying the Parseval's theorem to (2.46) by multiplying $\tilde{J}_{xm}(n)$ and $\tilde{J}_{zi}(n)$ to the first and

second, then perform the summation over n, we get:

$$\begin{pmatrix} K_{xx} & K_{xz} \\ K_{zx} & K_{zz} \end{pmatrix}\begin{pmatrix} A \\ B \end{pmatrix} = 0 \tag{2.55}$$

where

$$
\begin{aligned}
K_{xx}^{mi} &= \sum_{n=-\infty}^{\infty} \tilde{J}_{xm}(n) G_{xx}(n,\beta) \tilde{J}_{xi}(n) \\
K_{xz}^{mi} &= K_{zx}^{mi} = \sum_{n=-\infty}^{\infty} \tilde{J}_{xm}(n) G_{xz}(n,\beta) \tilde{J}_{zi}(n) \\
K_{zz}^{mi} &= \sum_{n=-\infty}^{\infty} \tilde{J}_{zm}(n) G_{zz}(n,\beta) \tilde{J}_{zi}(n) \\
A &= \left(I_{x1}, I_{x2}, ..., I_{xM}\right)' \qquad B = \left(I_{z1}, I_{z2}, ..., I_{zN}\right)' \\
m &= 1, 2, ..., M \qquad i = 1, 2, ..., N
\end{aligned} \tag{2.56}
$$

With the above matrix, the propagating constant can be solved from the eigenvalue

equation.

2.3.3 Eigen value problems

In the K matrix, the current expansion parameter A and B are unknowns. So we have

$M + N$ unknowns for current basis functions. To have non-trivial solution to (2.55), the

determinant of K matrix must be zero.

In the determinant of K matrix, the frequency and propagating constant are included. If

the frequency is given, propagating constant can be solved by the eigenvalue equation.

$$D(\beta, w) = \det \begin{pmatrix} K_{xx} & K_{xz} \\ K_{zx} & K_{zz} \end{pmatrix} = 0 \tag{2.57}$$

If the frequency is given, the initial guess of β can be used to find the root iteratively. Once the propagation constant is obtained, the normalized field and power can also be derived.

2.4 Field distributions

Once we get potentials expression in the spectral domain, the fields in spectral domain can also be derived. The inverse Fourier series summation is used.

Here, $\Phi_1^{(e)}(x, y)$ is even and $\Phi_1^{(h)}(x, y)$ is odd, according to x. Now, (2.22) is used to transfer the spectral domain field to spatial domain.

Region 1

$$
\begin{aligned}
\Phi_1^{(e)}(x, y) &= \frac{1}{a} \sum_{n=1}^{\infty} A(n) \sinh(\gamma_1 y) \cos(\alpha_n x) \\
\Phi_1^{(h)}(x, y) &= \frac{-j}{a} \sum_{n=1}^{\infty} C(n) \cosh(\gamma_1 y) \sin(\alpha_n x) \\
\frac{\partial}{\partial x} \Phi_1^{(e)}(x, y) &= \frac{-1}{a} \sum_{n=1}^{\infty} A(n) \sinh(\gamma_1 y) \alpha_n \sin(\alpha_n x) \\
\frac{\partial}{\partial x} \Phi_1^{(h)}(x, y) &= \frac{-j}{a} \sum_{n=1}^{\infty} C(n) \cosh(\gamma_1 y) \alpha_n \cos(\alpha_n x) \\
\frac{\partial}{\partial y} \Phi_1^{(e)}(x, y) &= \frac{1}{a} \sum_{n=1}^{\infty} A(n) \gamma_1 \cosh(\gamma_1 y) \cos(\alpha_n x) \\
\frac{\partial}{\partial y} \Phi_1^{(h)}(x, y) &= \frac{-j}{a} \sum_{n=1}^{\infty} C(n) \gamma_1 \sinh(\gamma_1 y) \sin(\alpha_n x)
\end{aligned}
\tag{2.58}
$$

Region 2

$$
\begin{aligned}
\Phi_2^{(e)}(x, y) &= \frac{1}{a} \sum_{n=1}^{\infty} B(n) \frac{\sinh\left[\gamma_2(h + d - y)\right]}{\sinh(\gamma_2 d)} \cos(\alpha_n x) \\
\Phi_2^{(h)}(x, y) &= \frac{-j}{a} \sum_{n=1}^{\infty} D(n) \frac{\cosh\left[\gamma_2(h + d - y)\right]}{\cosh(\gamma_2 d)} \sin(\alpha_n x)
\end{aligned}
$$

$$\frac{\partial}{\partial x}\Phi_2^{(e)}(x,y) = \frac{-1}{a}\sum_{n=1}^{\infty}B(n)\frac{\sinh\left[\gamma_2(h+d-y)\right]}{\sinh(\gamma_2 d)}\alpha_n\sin(\alpha_n x)$$

$$\frac{\partial}{\partial x}\Phi_2^{(h)}(x,y) = \frac{-j}{a}\sum_{n=1}^{\infty}D(n)\frac{\cosh\left[\gamma_2(h+d-y)\right]}{\cosh(\gamma_2 d)}\alpha_n\cos(\alpha_n x) \qquad (2.59)$$

$$\frac{\partial}{\partial y}\Phi_2^{(e)}(x,y) = \frac{1}{a}\sum_{n=1}^{\infty}B(n)\gamma_2\frac{\cosh\left[\gamma_2(h+d-y)\right]}{\sinh(\gamma_2 d)}\cos(\alpha_n x)$$

$$\frac{\partial}{\partial y}\Phi_2^{(h)}(x,y) = \frac{-j}{a}\sum_{n=1}^{\infty}D(n)\gamma_2\frac{\sinh\left[\gamma_2(h+d-y)\right]}{\cosh(\gamma_2 d)}\sin(\alpha_n x)$$

Substituting the above equations into (2.4), all of the field components at arbitrary position can be calculated.

2.5 Power flow

The total power flowing through the cross section of microstrip line can be calculated by the integrating the z component of complex Poynting vector $\left(\vec{E}\times\vec{H}^*\right)/2$ over the x-and y-direction [15]. By the Parseval's theorem, the spatial domain integral of complex Poynting vector can be transferred to spectral domain. In SDA, we already have all the field forms. Then the total power can be derived as:

$$P = \frac{1}{2}\int_0^{d+h}\int_{-a}^{a}\vec{E}\times\vec{H}^*\cdot\hat{z}dxdy = \frac{1}{4a}\sum_{n=-\infty}^{\infty}\int_0^{d+h}\left(\tilde{E}_{x,i}\tilde{H}_{y,i}^* - \tilde{E}_{y,i}\tilde{H}_{y,i}^*\right)dy \qquad (2.60)$$

where $*$ stands for the operator of complex conjugate.

With the expressions in (2.26), the field components of spectral domain can be written in the same forms.

$$\tilde{E}_{x1}(\alpha,y) = \left(-j\alpha A + \frac{\omega\mu_1\gamma_1}{\beta}C\right)\sinh(\gamma_1 y) \qquad (2.61)$$

$$\tilde{H}_{y1}(\alpha,y) = \left(C\gamma_1 - \frac{j\omega\varepsilon_1\alpha}{\beta}A\right)\sinh(\gamma_1 y) \qquad (2.62)$$

$$\tilde{E}_{y1}(\alpha, y) = \left(A\gamma_1 + \frac{j\alpha\omega\mu_1}{\beta}C \right)\cosh(\gamma_1 y) \tag{2.63}$$

$$\tilde{H}_{x1}(\alpha, y) = \left(-j\alpha C - \frac{\omega\varepsilon_1}{\beta}A\gamma_1 \right)\cosh(\gamma_1 y) \tag{2.64}$$

Multiplying the electric and magnetic fields, we come to

$$\begin{aligned}
\tilde{E}_{x1}(\alpha, y)\tilde{H}_{y1}^*(\alpha, y) &= K_A \sinh(\gamma_1 y)\sinh(\gamma_1^* y) \\
\tilde{E}_{y1}(\alpha, y)\tilde{H}_{x1}^*(\alpha, y) &= K_B \cosh(\gamma_1 y)\cosh(\gamma_1^* y)
\end{aligned} \tag{2.65}$$

where

$$\begin{aligned}
K_A &= \left(-j\alpha A + \frac{\omega\mu_1\gamma_1}{\beta}C \right)\left(C\gamma_1 - \frac{j\omega\varepsilon_1\alpha}{\beta}A \right)^* \\
K_B &= \left(A\gamma_1 + \frac{j\omega\mu_1\alpha}{\beta}C \right)\left(-j\alpha C - \frac{\omega\varepsilon_1}{\beta}A\gamma_1 \right)^*
\end{aligned}$$

Similarly, in region 2

$$\begin{aligned}
\tilde{E}_{x2}(\alpha, y)\tilde{H}_{y2}^*(\alpha, y) &= K_C \sinh\left[\gamma_2(h+d-y)\right]\sinh\left[\gamma_2^*(h+d-y)\right] \\
\tilde{E}_{y2}(\alpha, y)\tilde{H}_{x2}^*(\alpha, y) &= K_D \cosh\left[\gamma_2(h+d-y)\right]\cosh\left[\gamma_2^*(h+d-y)\right]
\end{aligned} \tag{2.66}$$

where

$$\begin{aligned}
K_C &= \left(\frac{-j\alpha B}{\sinh(\gamma_2 d)} - \frac{\omega\mu_2\gamma_2 D}{\beta\cosh(\gamma_2 d)} \right)\left(\frac{-D\gamma_2}{\cosh(\gamma_2 d)} - \frac{j\omega\varepsilon_2\alpha B}{\beta\sinh(\gamma_2 d)} \right)^* \\
K_D &= \left(\frac{-B\gamma_2}{\sinh(\gamma_2 d)} + \frac{j\alpha\omega\mu_2 D}{\beta\cosh(\gamma_2 d)} \right)\left(\frac{-j\alpha D}{\cosh(\gamma_2 d)} + \frac{\omega\varepsilon_2 B\gamma_2}{\beta\sinh(\gamma_2 d)} \right)^*
\end{aligned}$$

To simply the expressions, we rewrite the expression into exponential functions which show

In region 1,

$$\begin{aligned}
&\tilde{E}_{x1}(\alpha, y)\tilde{H}_{y1}^*(\alpha, y) - \tilde{E}_{y1}(\alpha, y)\tilde{H}_{x1}^*(\alpha, y) \\
&= K_A \sinh(\gamma_1 y)\sinh(\gamma_1^* y) - K_B \cosh(\gamma_1 y)\cosh(\gamma_1^* y) \\
&= \frac{1}{4}\left[(K_A - K_B)\left(e^{2R_1 y} + e^{-2R_1 y}\right) - (K_A + K_B)\left(e^{2jI_1 y} + e^{-2jI_1 y}\right) \right]
\end{aligned} \tag{2.67}$$

In region 2

$$\tilde{E}_{x2}(\alpha, y)\tilde{H}_{y2}^*(\alpha, y) - \tilde{E}_{y2}(\alpha, y)\tilde{H}_{x2}^*(\alpha, y)$$

$$= K_C \sinh(\gamma_2 L)\sinh(\gamma_2^* L) - K_D \cosh(\gamma_2 L)\cosh(\gamma_2^* L)$$

$$= \frac{1}{4}\left[(K_C - K_D)(e^{2R_2 L} + e^{-2R_2 L}) - (K_C + K_D)(e^{2jI_2 L} + e^{-2jI_2 L})\right] \tag{2.68}$$

where

$$R_1 = Re(\gamma_1) \qquad R_2 = Re(\gamma_2)$$

$$I_1 = Im(\gamma_1) \qquad I_2 = Im(\gamma_2)$$

$$L = h + d - y$$

With the field expression in the spectral domain, now we can get the integral over y-direction. By rewriting the integrand in the exponential forms, the integral can be written in the close form. For the two regions, we split the integral into two parts.

Region 1:

$$P_1(\alpha) = \int_0^h \left[\tilde{E}_{x1}(\alpha, y)\tilde{H}_{y1}^*(\alpha, y) - \tilde{E}_{y1}(\alpha, y)\tilde{H}_{x1}^*(\alpha, y)\right]dy$$

$$= \int_0^h \left[K_A \sinh(\gamma_1 y)\sinh(\gamma_1^* y) - K_B \cosh(\gamma_1 y)\cosh(\gamma_1^* y)\right]dy$$

$$= \frac{1}{4}\int_0^h \left[(K_A - K_B)(e^{2R_1 y} + e^{-2R_1 y}) - (K_A + K_B)(e^{2jI_1 y} + e^{-2jI_1 y})\right]dy$$

$$= \frac{1}{4}\left[(K_A - K_B)\left(\frac{e^{2R_1 h} - e^{-2R_1 h}}{2R_1}\right) - (K_A + K_B)\left(\frac{e^{2jI_1 h} - e^{-2jI_1 h}}{2I_1 j}\right)\right] \tag{2.69}$$

Region 2:

$$P_2(\alpha) = \int_h^{h+d} \left[\tilde{E}_{x2}(\alpha, y)\tilde{H}_{y2}^*(\alpha, y) - \tilde{E}_{y2}(\alpha, y)\tilde{H}_{x2}^*(\alpha, y)\right]dy$$

$$= \int_d^0 \left[K_C \sinh(\gamma_2 L)\sinh(\gamma_2^* L) - K_B \cosh(\gamma_2 L)\cosh(\gamma_2^* L)\right]dL$$

$$= -\frac{1}{4}\int_d^0 \left[(K_C - K_D)(e^{2R_2 L} + e^{-2R_2 L}) - (K_C + K_D)(e^{2jI_2 L} + e^{-2jI_2 L})\right]dL$$

$$= \frac{1}{4}\left[(K_C - K_D)\left(\frac{e^{2R_2 d} - e^{-2R_2 d}}{2R_2}\right) - (K_C + K_D)\left(\frac{e^{2jI_2 d} - e^{-2jI_2 d}}{2I_2 j}\right)\right] \tag{2.70}$$

Now we get the integral of the spectral domain fields over y, then the total power can

be calculated through the series summation

$$P = \frac{1}{2}\int_0^{d+h}\int_{-a}^{a} \bar{E} \times \bar{H}^* \cdot \hat{z}\, dx\, dy = \frac{1}{2a}\sum_{n=1}^{\infty}\left[P_1(\alpha_n) + P_2(\alpha_n)\right]$$

(2.71)

CHAPTER 3. NUMERICAL CONSIDERATION AND RESULTS

In Chapter 2, the spectral domain analysis of shield microstrip is conducted. For the open microstrip with DNG metamaterials is provided in Appendix A. In this chapter, we focus on the numerical implementation of the spectrum domain approach. In order to improve the numerical efficiency, several acceleration techniques are introduced, which are implemented in the numerical calculation. For the microstrip, the dispersion properties are studied over a frequency range from 1GHz to 100GHz with different geometric setups and terms of current basis functions. Based on the dispersion results, the field distribution, total power, and characteristic impedance can be calculated.

3.1 Numerical acceleration techniques

In the spectral domain method of open microstrip line, as the frequency increases and the structure becomes complicated, the convergence of the integral tends to be slow. The spectral domain approach successfully renders rigorous solution at the expense of higher computation cost.

In [16], several numerical speeding techniques are introduced. In this thesis, these methods are also included, which are implemented in the numerical calculation.   The computation time is significantly reduced with a high accuracy.

3.1.1 Integral range reduction

In method of moments, the Galerkin's method and Parseval's theorem are applied to derive the eigenvalue equation. To get the K matrix, summation/integral over α from $-\infty$ to ∞ needs to be performed, which is in (2.56).

Here we can do to reduce the computation cost by cutting to half. In spectral

domain, $\tilde{J}_z(\alpha)$, $G_{xx}(\alpha,\beta)$, and $G_{zz}(\alpha,\beta)$ are even functions of α, while $\tilde{J}_x(\alpha)$, $G_{xz}(\alpha,\beta)$,

and $G_{zx}(\alpha,\beta)$ are odd functions. So the integrand of K matrix elements are always even

functions.

For open microstrip lines, due to the properties of symmetric integral of even functions,

we can use the following integrals instead of the previous ones.

$$
\begin{aligned}
K_{xx}^{mn} &= 2\int_0^\infty \tilde{J}_{xm}(\alpha)G_{xx}(\alpha,\beta)\tilde{J}_{xn}(\alpha)\,d\alpha \\
K_{xz}^{mn} &= K_{zx}^{nm} = 2\int_0^\infty \tilde{J}_{xm}(\alpha)G_{xz}(\alpha,\beta)\tilde{J}_{zn}(\alpha)\,d\alpha \\
K_{zz}^{mn} &= 2\int_0^\infty \tilde{J}_{zm}(\alpha)G_{zz}(\alpha,\beta)\tilde{J}_{zn}(\alpha)\,d\alpha
\end{aligned}
\tag{3.1}
$$

The above integrals can reduce the range by half, which will significantly improve the

calculation efficiency. For shielded microstrip line, we can use the same technique to cut the

summation time.

3.1.2 Symmetry of K Matrix

In the numerical implementation, filling K matrix elements is always time consuming.

The decrease of the size can directly reduce the time consumption.

In the K matrix, we find that the K_{xx} and K_{zz} have the symmetric properties. (3.1)

implies that

$$
\begin{aligned}
K_{xx}^{mn} &= K_{xx}^{nm} \\
K_{zz}^{mn} &= K_{zz}^{nm}
\end{aligned}
\tag{3.2}
$$

So we only need to calculate the elements with $i = 1,...,M$ and $j = i,...,M$. It means that

we only need to calculate the upper triangular matrix of the K_{xx} , K_{zz} .

In addition, we have

$$K_{xz}^{mn} = K_{zx}^{nm} = 2\int_0^\infty \tilde{J}_{xm}(\alpha)G_{xz}(\alpha,\beta)\tilde{J}_{zn}(\alpha)d\alpha. \tag{3.3}$$

Combining (3.2) and (3.3), we can conclude that

$$K_{xz} = \left(K_{zx}\right)^T \tag{3.4}$$

Here, it is obvious that we only need to calculate the upper triangular matrix of K matrix.

3.1.3 Leading term extraction

3.1.3.1 Close form identity

In the case of open microstrip lines, for each element of the K matrix, the integral of two multiplying Bessel functions over α is included. If we directly calculate the integral, the convergence is very slow and a huge amount of CPU time is needed to get accurate results. The leading term extraction technique is one of the techniques that can be applied to reduce the CPU time for the integrals.

In [18, 19, 20], following integral can expressed as the close form.

$$\int_0^\infty \frac{x}{x^2+y^2}J_{2m}(ax)J_{2n}(ax)dx = (-1)^{m-n}I_{2m}(ay)K_{2n}(ay) \tag{3.5}$$

in which $Re(y) > 0$ and $2m > 2n-2$. $I_n(x)$ and $K_n(x)$ are the modified Bessel function of the first and second kind. The identity is good except for negative real y^2. When y^2 is purely negative, there will be a pole in the integral path at $|y|$. If we take the residue of the pole into consideration, then the identity is still valid [16].

$$\int_0^\infty \frac{x}{x^2+y^2} J_{2m}(ax) J_{2n}(ax) dx$$

$$= \lim_{\varepsilon \to 0} \left[\int_0^{|y|-\varepsilon} + \int_{|y|+\varepsilon}^\infty \right] dx \frac{x}{x^2+y^2} J_{2m}(ax) J_{2n}(ax) - \frac{\pi j}{2} J_{2m}(a|y|) J_{2n}(a|y|)$$

$$= (-1)^{m-n} I_{2m}(ay) K_{2n}(ay) \tag{3.6}$$

The above identity can be used in the leading extraction for the K matrix element calculation for the open microstrip line.

3.1.3.2 Leading term conditions

The asymptotic forms of some expressions need to be derived to perform leading term extraction. As $\alpha \to \infty$, we find that the γ_i can be approximated as the first two terms of their Taylor expansion.

$$\gamma_i = \sqrt{\alpha^2 + \beta^2 - k_i^2} \approx |\alpha| + \frac{\beta^2 - k_i^2}{2|\alpha|} \tag{3.7}$$

Once the condition is met, leading term can be extracted. First, we extract the leading term for the denominator in (2.47).

$$\tilde{\Delta} = \left[\varepsilon_r \gamma_2 + \gamma_1 \tanh(\gamma_1 h) \right] \left[\mu_r \gamma_2 + \gamma_1 \coth(\gamma_1 h) \right] \approx (\varepsilon_r \gamma_2 + \gamma_1)(\mu_r \gamma_2 + \gamma_1)$$

$$\approx \alpha^2 (1+\varepsilon_r)(1+\mu_r) + \frac{1}{2}(1+\varepsilon_r)\left[(\beta^2 - k_1^2) + \mu_r (\beta^2 - k_2^2) \right] \tag{3.8}$$

$$+ \frac{1}{2}(1+\mu_r)\left[(\beta^2 - k_1^2) + \varepsilon_r (\beta^2 - k_2^2) \right]$$

3.1.3.3 Kxx

With the leading term extraction on the Green's function, we are able to improve the convergence of K matrix. The derivation of the following leading terms extractions can be found in [16]. All the following Green's functions are normalized to $j\eta_2/k_2$.

Once the leading term is obtained in desired form, the identity in (3.6) can be used to get the close form for the integral.

$$G_{xx}(\alpha,\beta)=\frac{1}{\tilde{\Delta}}\Big[\gamma_2(\alpha^2-k_1^2)+\mu_r\gamma_1(\alpha^2-k_2^2)\tanh(\gamma_1h)\Big]\approx\frac{\alpha^3}{(1+\varepsilon_r)}\frac{1}{\alpha^2+y_{xx}^2}\qquad(3.9)$$

in which

$$y_{xx}^2=\frac{\beta^2(1+\varepsilon_r)+k_2^2+\varepsilon_rk_1^2}{2(1+\varepsilon_r)}\ .\qquad(3.10)$$

Thus the element of matrix is

$$\begin{aligned}K_{xx}^{mn}&=\int_0^\infty\tilde{J}_{xm}(\alpha)G_{xx}(\alpha,\beta)\tilde{J}_{xm}(\alpha)d\alpha\\&=4\pi^2mn(-1)^{m+n}\int_0^\infty\alpha^{-2}J_{2m}(\delta)\Bigg[G_{xx}(\alpha,\beta)-\frac{\alpha^3}{(1+\varepsilon_r)}\frac{1}{\alpha^2+y_{xx}^2}\Bigg]J_{2n}(\delta)d\alpha\\&\quad+4\pi^2mn(-1)^{m+n}\frac{(-1)^{m-n}}{(1+\varepsilon_r)}I_{\max\{2m,2n\}}\left(\frac{wy_{xx}}{2}\right)K_{\max\{2m,2n\}}\left(\frac{wy_{xx}}{2}\right).\end{aligned}\qquad(3.11)$$

3.1.3.4 Kxz

$$G_{xz}(\alpha,\beta)=\frac{\alpha\beta}{\tilde{\Delta}}\Big[\gamma_2+\mu_r\gamma_1\tanh(\gamma_1h)\Big]\approx\frac{\beta}{(1+\varepsilon_r)}\frac{\alpha^2}{\alpha^2+y_{xz}^2}\qquad(3.12)$$

in which

$$y_{xz}^2=\frac{\beta^2}{2}+\frac{-2k_1^2-\varepsilon_rk_1^2-\mu_rk_2^2-2\varepsilon_r\mu_rk_2^2+k_2^2+\varepsilon_r\mu_rk_1^2}{2(1+\mu_r)(1+\varepsilon_r)}\ .\qquad(3.13)$$

Then

$$\begin{aligned}K_{xz}^{mn}&=\int_0^\infty\tilde{J}_{xm}(\alpha)G_{xz}(\alpha,\beta)\tilde{J}_{zn}(\alpha)\\&=-\pi^2wm(-1)^{m+n}\left\{\int_0^\infty J_{2m}\left(\frac{\alpha w}{2}\right)\Bigg[\alpha^{-1}G_{xz}(\alpha,\beta)-\frac{\beta}{1+\varepsilon_r}\frac{\alpha^2}{\alpha^2+y_{xz}^2}\Bigg]J_{2n-2}\left(\frac{\alpha w}{2}\right)d\alpha\right\}\\&\quad+\pi^2wm\frac{\beta}{(1+\varepsilon_r)}I_{\max\{2m,2n-2\}}\left(\frac{\omega y_{xz}}{2}\right)K_{\max\{2m,2n-2\}}\left(\frac{\omega y_{xz}}{2}\right).\end{aligned}\qquad(3.14)$$

3.1.3.5 Kzz

$$G_{zz}(\alpha,\beta) = \frac{1}{\Delta}\Big[\gamma_2\big(\beta^2 - k_1^2\big) + \mu_r\gamma_1\big(\beta^2 - k_2^2\big)\tanh(\gamma_1 h)\Big] \approx \frac{\big(\beta^2 - k_1^2\big) + \mu_r\big(\beta^2 - k_2^2\big)}{(1+\varepsilon_r)(1+\mu_r)}\frac{\alpha}{\alpha^2 + y_{zz}^2} \qquad (3.15)$$

in which

$$y_{zz}^2 = \frac{1}{2}\left[\frac{\big(\beta^2 - k_1^2\big) + \mu_r\big(\beta^2 - k_2^2\big)}{(1+\mu_r)} + \frac{\big(\beta^2 - k_1^2\big) + \varepsilon_r\big(\beta^2 - k_2^2\big)}{(1+\varepsilon_r)} - \frac{\big(\beta^2 - k_2^2\big)\big(\beta^2 - k_1^2\big)(1+\mu_r)}{\big(\beta^2 - k_1^2\big) + \mu_r\big(\beta^2 - k_2^2\big)}\right]. \qquad (3.16)$$

So

$$\begin{aligned}
K_{zz}^{mn} &= \int_0^\infty \tilde{J}_{zm}(\alpha)G_{zz}(\alpha,\beta)\tilde{J}_{zn}(\alpha)d\alpha \\
&= \frac{\pi^2 w^2}{4}(-1)^{m+n}\int_0^\infty J_{2m-2}\left(\frac{\alpha w}{2}\right)\left\{G_{zz}(\alpha,\beta) - \frac{\big(\beta^2 - k_1^2\big) + \mu_r\big(\beta^2 - k_2^2\big)}{(1+\varepsilon_r)(1+\mu_r)}\frac{\alpha}{\alpha^2 + y_{zz}^2}\right\}J_{2n-2}\left(\frac{\alpha w}{2}\right)d\alpha \\
&\quad + \frac{\pi^2 w^2}{4}\frac{\big(\beta^2 - k_1^2\big) + \mu_r\big(\beta^2 - k_2^2\big)}{(1+\varepsilon_r)(1+\mu_r)}I_{\max\{2m-2,2n-2\}}\left(\frac{wy_{zz}}{2}\right)K_{\max\{2m-2,2n-2\}}\left(\frac{wy_{zz}}{2}\right).
\end{aligned} \qquad (3.17)$$

After the leading term extraction, we list the new convergence speed according to α in Table 1 [16].

Table 1. Convergence comparison of K matrix element and Green's functions before and after leading term (LE) extraction.

	G_{xx}	K_{xx}	G_{xz}	K_{xz}	G_{zz}	K_{zz}
After LE	α^{-3}	α^{-6}	α^{-4}	α^{-6}	α^{-5}	α^{-6}
Before LE	α	α^{-2}	1	α^{-2}	α^{-1}	α^{-2}

Before the leading term extraction, the convergence of K_{pq} is proportional to α^{-2}. After leading term, the convergence of K_{pq} has four order improvements. So leading term extraction of Green's functions will improve the numerical calculation efficiency significantly.

3.2 Shielded microstrip numerical results

3.2.1 Dispersion property

In this part, numerical scripts of spectral domain method (SDA) are used to analyze the properties of the shielded microstrip. Fig. 2.1 shows the structures of the shielded microstrip lines. In [21], Krowne published his results of shielded microstrip line with DNG metamaterials. The normalized propagation constant $\gamma_z = (\alpha + j\beta)/k_0$ is calculated by the SDA in the frequency range from 1 GHz to 100 GHz.

First, in order to compare with published results, the shielded microstrip line is studied, with air above the strip and DNG materials below with $\varepsilon_r = -2.5$ and $\mu_r = -2.5$, substrate thickness $h = 0.5$ mm, microstrip width $w = 0.5$ mm, two side wall distance $2a = 10h$ mm, air region height $d = 10h$. Fig. 3.1 shows the dispersion curves for shielded microstrip line. Our numerical results (blue lines) match very well with Krowne's (red points).

In Fig 3.1, the solid blue line is α and dashed blue line is β. One should notice that below 6 GHz, α is zero, so complex propagation constant is purely imaginary with one branch. In this region, the mode is purely propagating without attenuation. In the frequency range from 6 GHz to 75 GHz, α is not zero, so complex mode occurs, which will cause the wave to be evanescent in z -direction. Above 75 GHz, two branches begin to appear at the point where α drops to zero, so two purely propagating modes in z-direction occur in this region.
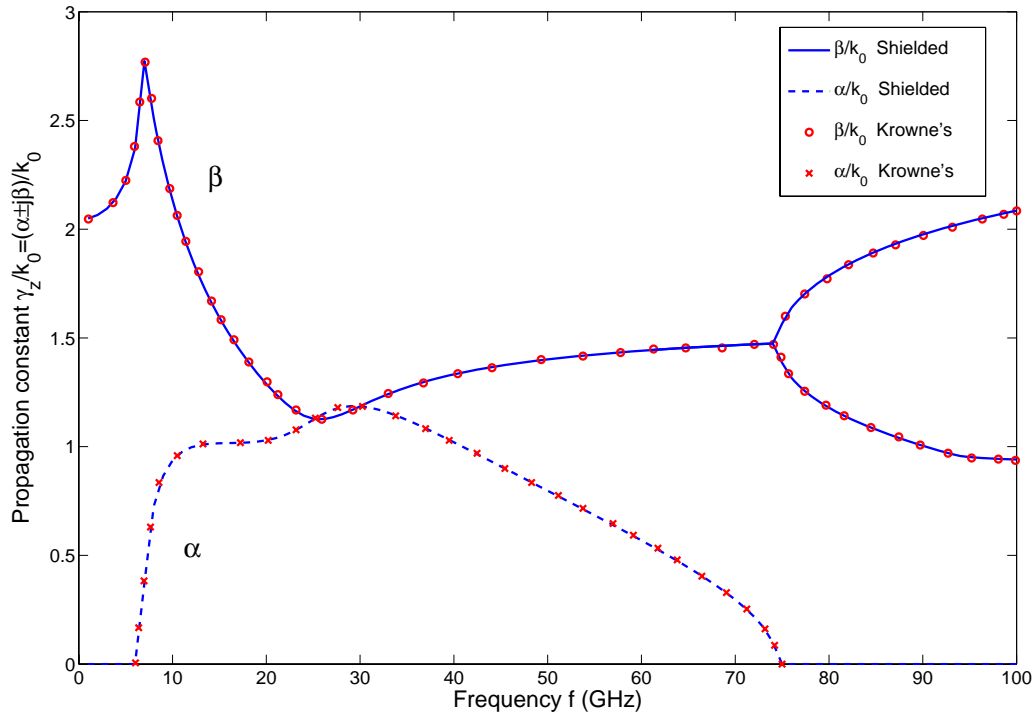
Figure 3.1 The shielded dispersion curves compared to Krowne's results with the same model setup using spectrum domain approach. The shielded microstrip line is filled with air above the strip and double negative materials $\left(\varepsilon_r = \mu_r = -2.5\right)$ below the strip, substrate thickness $h = 0.5\,\text{mm}$, strip width $w = 0.5\,\text{mm}$, two side wall distance $2a = 10h$, air region top wall height $d = 10h$.

 To know the effect of PEC boundary conditions, we change the geometric setup. Fig. 3.2 shows the dispersion curves for the microstrip line with two side PEC walls but the top PEC layer has been removed, which can be treated as $d = \infty$. The shielded result is also shown. From Fig. 3.2, one notices that large d will not change the dispersion too much.
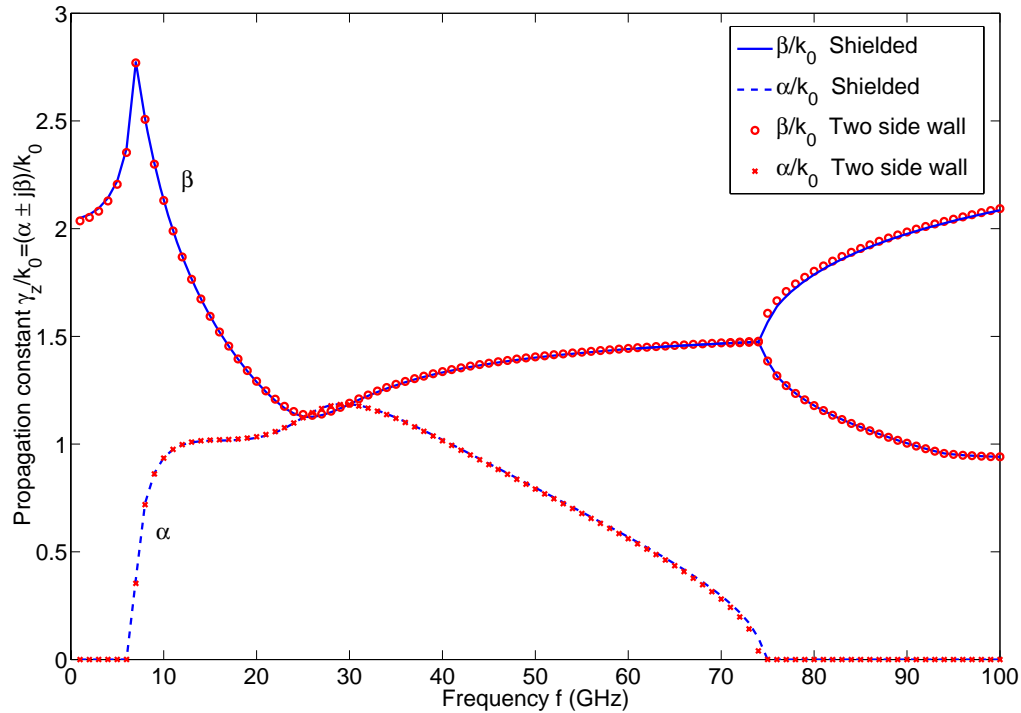
Figure 3.2 The dispersion curves of microstrip with two side walls compared to the shielded microstrip line with $d = 10h$. The shielded microstrip line is filled with air above the strip and double negative materials $\left(\varepsilon_r = \mu_r = -2.5\right)$ below the strip, substrate thickness $h = 0.5\,\text{mm}$, strip width $w = 0.5\,\text{mm}$, two side wall distance $2a = 10h$.

Then we decrease the d and try to see the difference. Fig 3.3 shows the dispersion curves for the same shielded microstrip model, but changing the distance d between strip and top PEC layer. As d decreases, the peaks of α and β are moving left and up. Moreover, the frequency range of the purely propagating mode at low frequency end is decreasing. However, above 40 GHz, we do not see significant changes according to d.

Figure 3.3 The dispersion curves of three shielded microstrip lines with DNG metamaterials, which are filled with air above the strip and double negative materials $\left(\varepsilon_r = \mu_r = -2.5\right)$ below the strip, substrate thickness $h = 0.5$ mm, strip width $w = 0.5$ mm, two side wall distance $2a = 10h$. $d = 10h$, $d = 5h$, $d = 4h$.

If d is decreased further, the disappearance of purely propagating mode at the low frequency is expected. Fig 3.4 shows the dispersion curves of the shielded microstrip with $d = 3.35h$ and $d = 3.3h$.
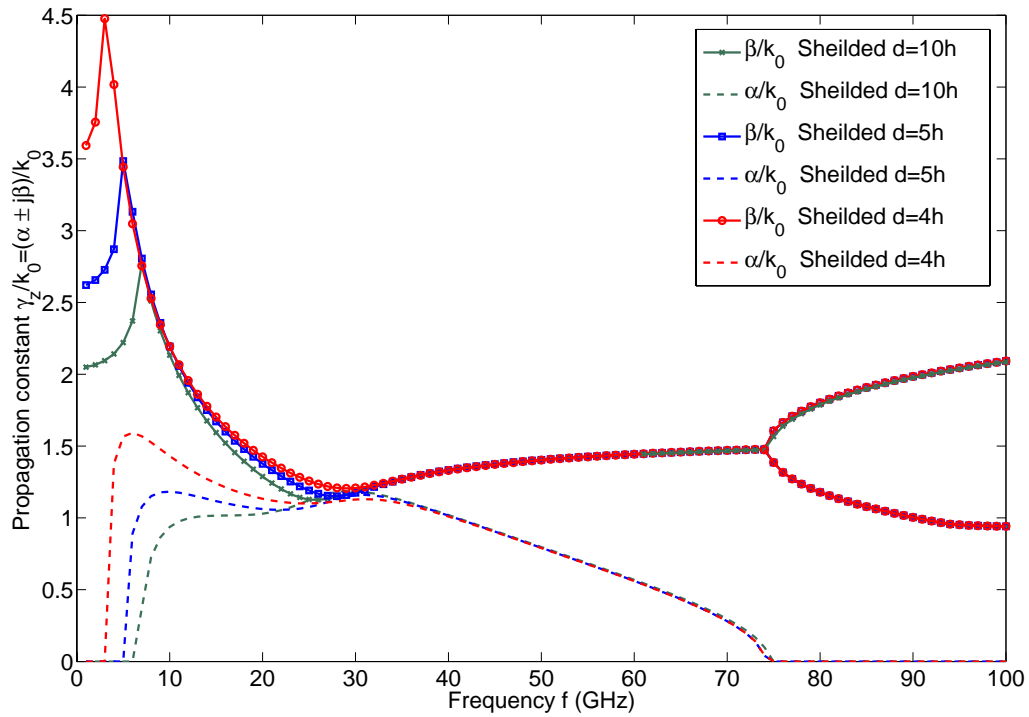
Figure 3.4 The dispersion curves of three shielded microstrip lines with DNG metamaterials, which are filled with air above the strip and double negative materials $\left(\varepsilon_r = \mu_r = -2.5\right)$ below the strip, substrate thickness $h = 0.5$ mm, strip width $w = 0.5$ mm, two side wall distance $2a = 10h$. $d = 10h$, $d = 3.35h$, $d = 3.3h$.

For $d = 3.35h$, below 1.6 GHz, purely propagating mode still exists, but the peak is high and at around 0.4 GHz. Above 40 GHz, the propagating curves match well with $d = 10h$. As d decrease to 3.3h, there is no propagating mode occurs below 10 GHz. α and β decrease, as frequency increases to 40 GHz. Above 40 GHz, the dispersion curves nearly keep same with that of the previous model.

Fig 3.5 shows the dispersion curves for $a = 4h, d = 10h$. Similarly, as a decreases, the purely propagating mode at low frequency is moving left.
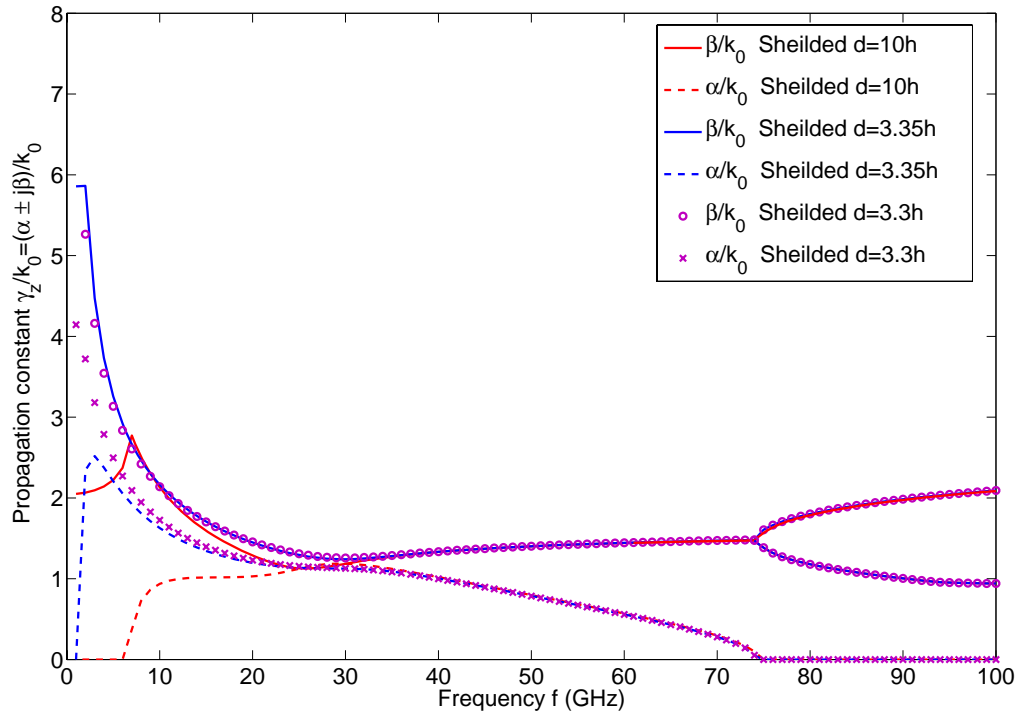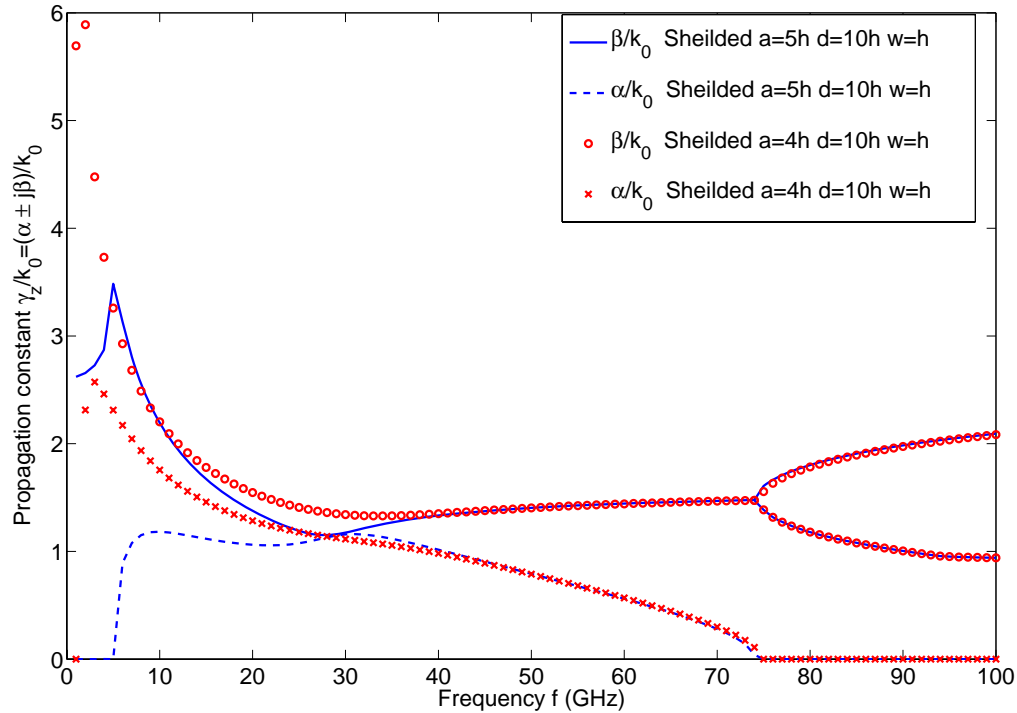

Figure 3.5 The dispersion curves of two shielded microstrip lines with DNG metamaterials, which are filled with air above the strip and double negative materials $(\varepsilon_r = \mu_r = -2.5)$ below the strip, substrate thickness $h = 0.5$ mm, strip width $w = 0.5$ mm, two side wall distance $a = 5h$ and $a = 4h$, air region PEC wall height $d = 10h$.

In the spectral domain analysis of shielded microstrip line, the K matrix element includes the multiplying of two current basis functions. The result accuracy of the spectrum domain approach is dictated by the number of basis functions which also determinates the size

of K matrix, the summation tolerance and the root searching accuracy. For high accuracy, the price paid is the computation cost, which, however, can be leveraged by applying numerical speeding methods, such as leading term extraction, high order integral rule, extrapolation, etc.

In Chapter 2, the unknown current distribution is expanded with Chebyshev polynomials with unknown coefficients. An accurate estimate of the current distribution requires more terms of polynomials, which will result in slow convergence.

Table 2.   Convergence of γ_z over different terms of Chebyshev polynomials for shielded microstrip line with $a = 5h, d = 10h, w = h, \varepsilon_r = \mu_r = -2.5$ at 10 GHz

$M \times N$	$\gamma_z = (\alpha \pm j\beta)/k_0$
1×1	$2.126446 \pm 0.931124\,j$
2×2	$2.126239 \pm 0.931385\,j$
3×3	$2.126239 \pm 0.931385\,j$
4×4	$2.126239 \pm 0.931385\,j$
5×5	$2.126239 \pm 0.931385\,j$
6×6	$2.126239 \pm 0.931385\,j$
7×7	$2.126239 \pm 0.931385\,j$
8×8	$2.126239 \pm 0.931385\,j$

In Table 2, we use the same summation accuracy control, root searching tolerance etc. It shows the convergence test for different number of terms of the Chebyshev polynomials being used. From the table, $M = N = 2$ is sufficient enough to make the result converge to high accuracy.

3.2.2 Field and power distributions

[21, 22] show the field distribution plot of the transverse electric E field vector (arrow length denotes magnitude) overlaid on the electric-field magnitude throughout the LHM.

In Chapter 2, we derive the field in spatial domain. If frequency is given, the propagation constant can be solved from the eigenvalue equation. Then with the propagating constant, the field distribution at any position can be calculated.

3.2.2.1 Propagating mode at 5GHz

Fig. 3.6 and Fig. 3.7 show the electric and magnetic field of shielded microstrip line with $a = 5h, d = 10h, w = h, \varepsilon_r = \mu_r = -2.5$ at 5GHz. In Fig 3.6, at the interface of air and DNG metamaterial, the electric fields in the two regions point away from the interface.

At the interface away from the strip, where $x > w/2$, the boundary conditions yields:

$$\hat{y} \cdot \left(\bar{D}_2 - \bar{D}_1 \right) = 0$$
$$\hat{y} \times \left(\bar{E}_2 - \bar{E}_1 \right) = 0 \tag{3.18}$$

Using the constitutive relationship, the above equations can be rewritten as :

$$\varepsilon_{r1} E_{n1} = \varepsilon_{r2} E_{n2}$$
$$E_{t1} = E_{t2} \tag{3.19}$$

where $\varepsilon_{r1} = -2.5, \varepsilon_{r2} = 1$

Thus the normal electric fields must be in different directions, which mean that they point away and toward the interface simultaneously.

In Fig 3.7, the magnetic field in the regions away from the strip also point away (left) and toward (right) the interface. Similarly, the boundary conditions for magnetic fields yield:

$$\hat{y} \cdot \left(\vec{B}_2 - \vec{B}_1 \right) = 0$$
$$\hat{y} \times \left(\vec{H}_2 - \vec{H}_1 \right) = 0$$
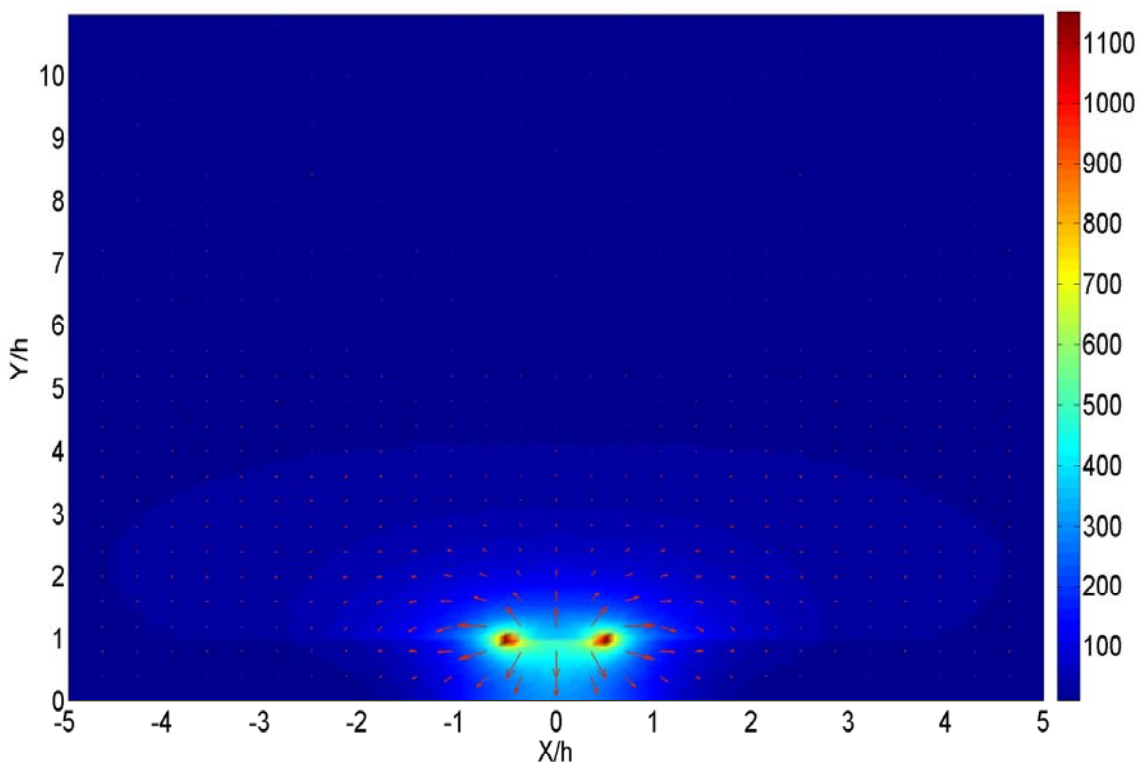
(3.20)

Figure 3.6 Electric field vector plot overlaid on electric field magnitude for shielded

microstrip line with $a = 5h, d = 10h, w = h, \varepsilon_r = \mu_r = -2.5$ at 5 GHz

Using the constitutive relationship, the above equations can be rewritten as :

$$\mu_{r1} B_{n1} = \mu_{r2} B_{n2}$$
$$H_{t1} = H_{t2}$$

(3.21)

where $\mu_{r1} = -2.5, \mu_{r2} = 1$

Thus the magnetic fields must point away and toward the interface simultaneously and the tangential magnetic field is continuous at the interface of air and DNG metamaterials.
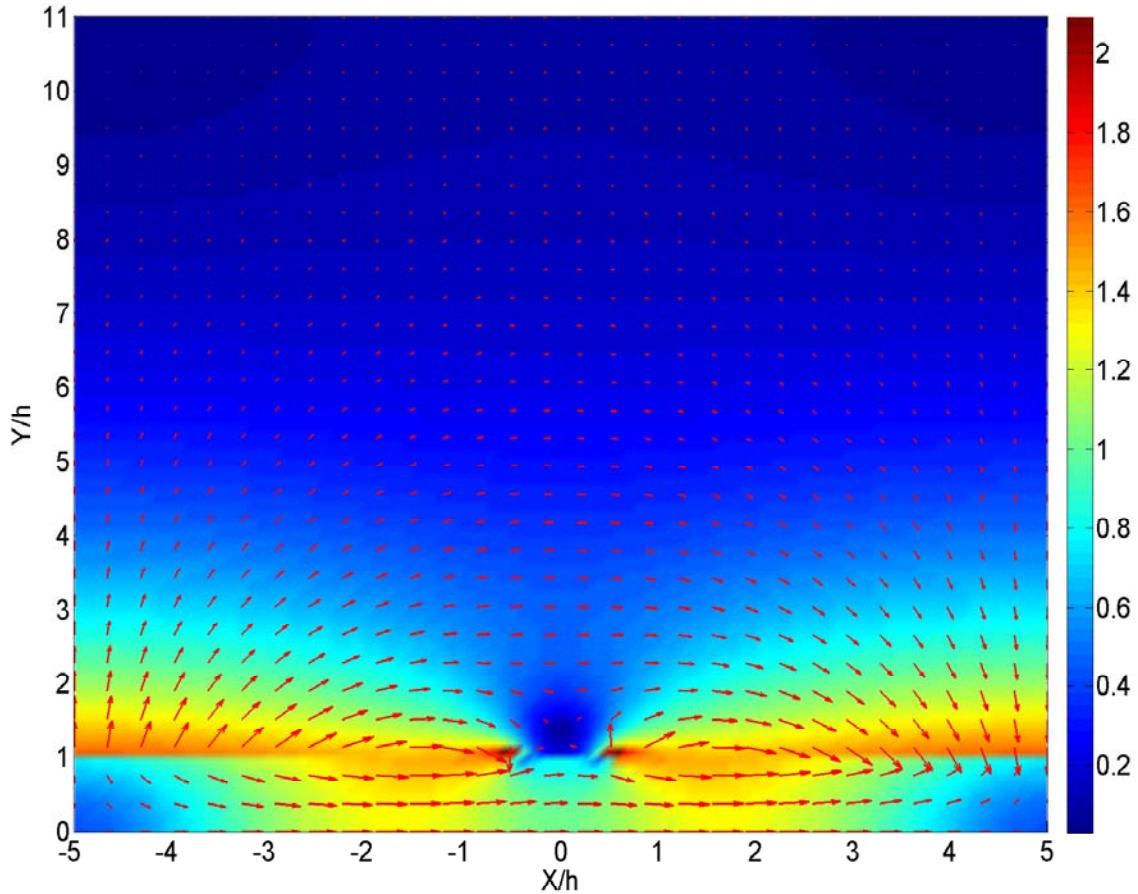

Figure 3.7 Magnetic field vector plot overlaid on magnetic field magnitude for shielded microstrip line with $a = 5h, d = 10h, w = h, \varepsilon_r = \mu_r = -2.5$ at 5 GHz

Figure 3.8 is the color plot of the Poynting vector $(-P_z)$ in the cross section of shielded microstrip line. So

$$P_z = \left(\vec{E}_t \times \vec{H}_t \right) \cdot \hat{z} = E_x H_y - E_y H_x \tag{3.22}$$

In Fig. 3.8, one notes that the total power is negative. Negative power occurs beneath the signal strip. Positive power only exists in the region near the edges of the strip.

Figure 3.8 Color plot of the longitudinal Poynting vector in the corss section of microstrip line with $a = 5h, d = 10h, w = h, \varepsilon_r = \mu_r = -2.5$ at 5 GHz (actually -Pz is plotted)

3.2.2.2 Complex mode at 10GHz

Fig. 3.9 and Fig. 3.10 show the electric and magnetic field of shielded microstrip line with $a = 5h, d = 10h, w = h$, $\varepsilon_r = \mu_r = -2.5$ at 10 GHz. The boundary conditions at the interface are still met.

In Fig. 3.9, the electric field distribution is similar to that of the propagating mode.
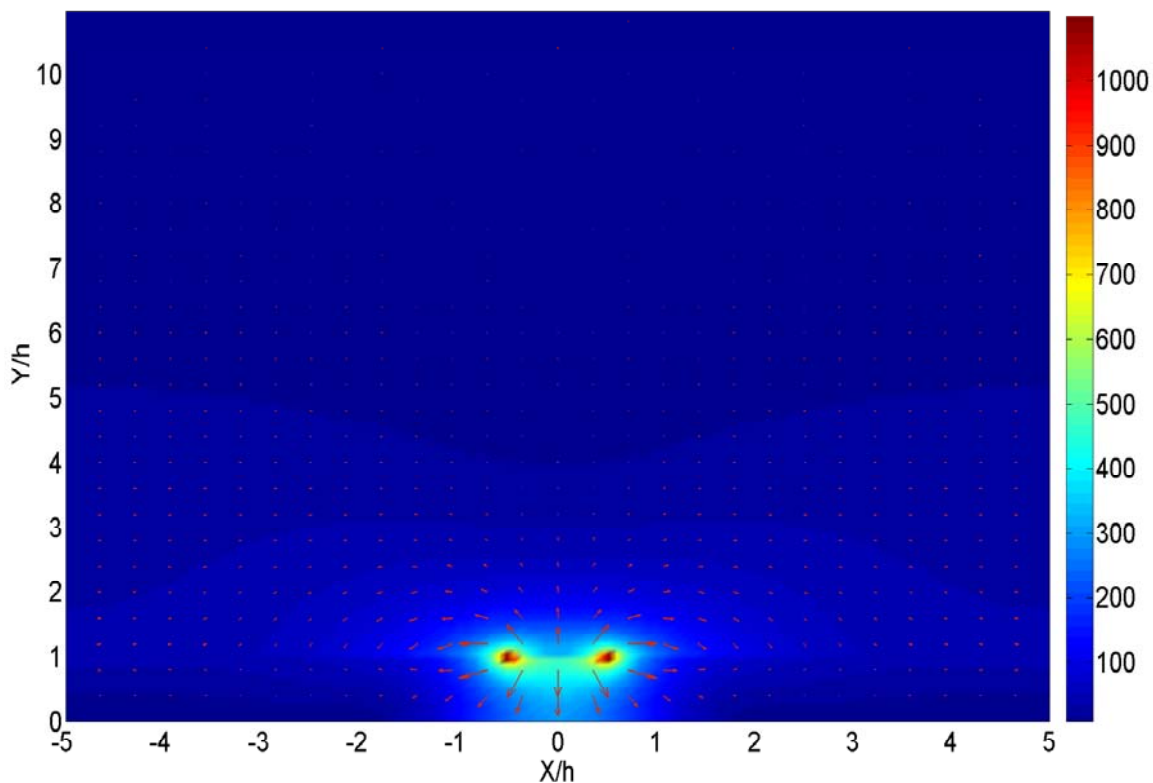
Figure 3.9 Electric field vector plot overlaid on electric field magnitude for shielded microstrip line with $a = 5h, d = 10h, w = h, \varepsilon_r = \mu_r = -2.5$ at 10 GHz

In Fig 3.10, the magnetic field is slightly different in the region away thestrip from the case of 5 GHz. One notes that the magnitude of magnetic field is large near the two side walls. The largest magnetic field is at the edges of the signal strip.
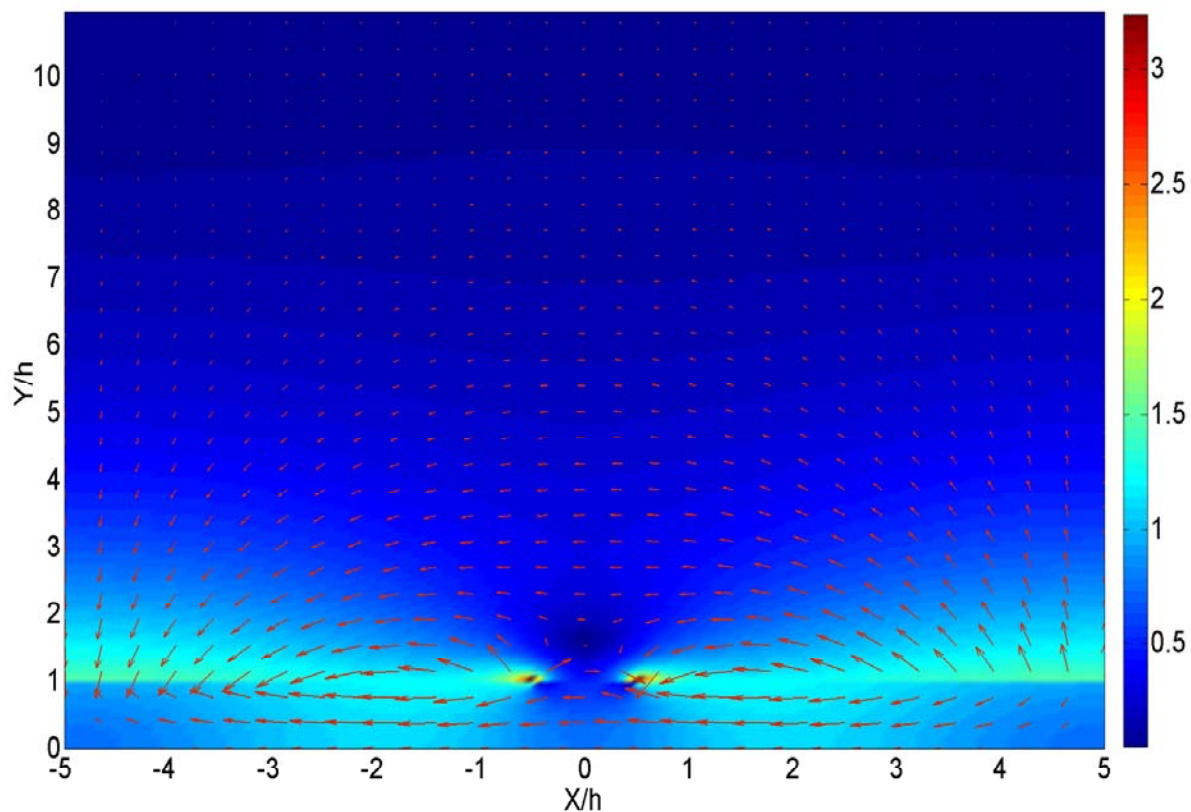
Figure 3.10 Magnetic field vector plot overlaid on magnetic field magnitude for shielded microstrip line with $a = 5h, d = 10h, w = h, \varepsilon_r = \mu_r = -2.5$ at 10 GHz

In Fig 3.11, the pointing power is plotted. Negative power is found beneath the strip and the region near strip in air. Positive power is found at the interface near the strip. The physical meaning of complex mode requires that the total power in the cross section is zero.
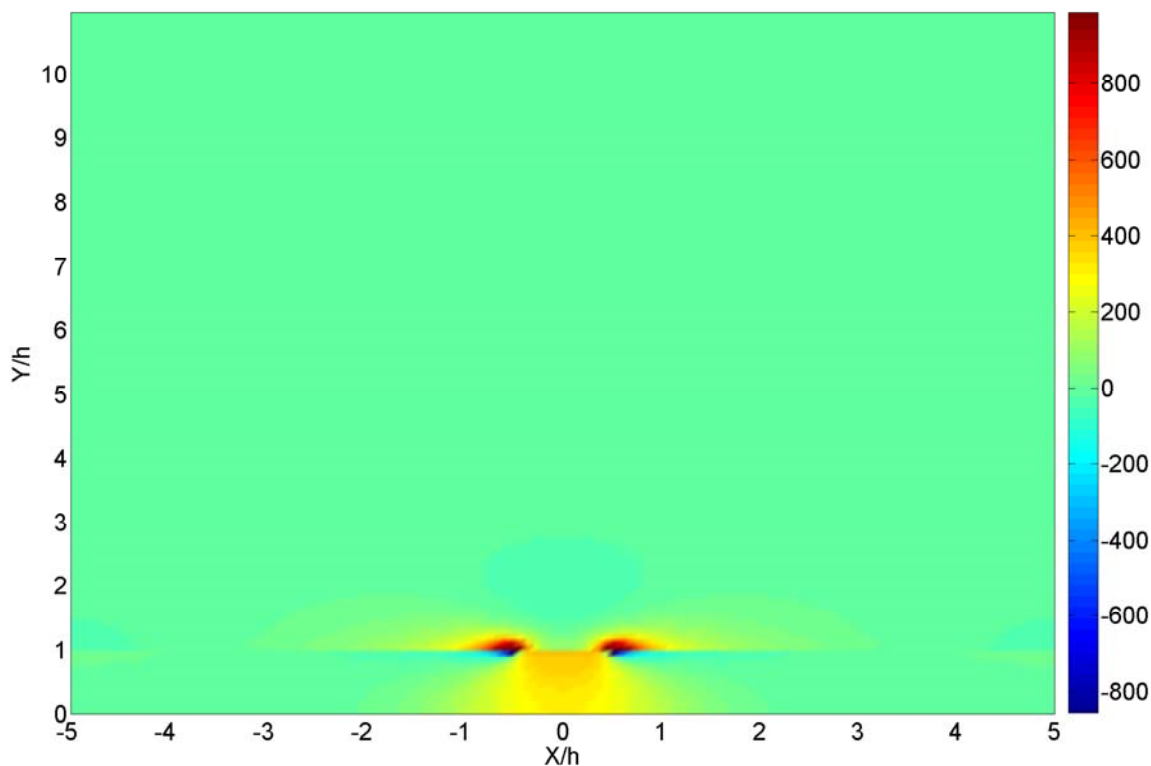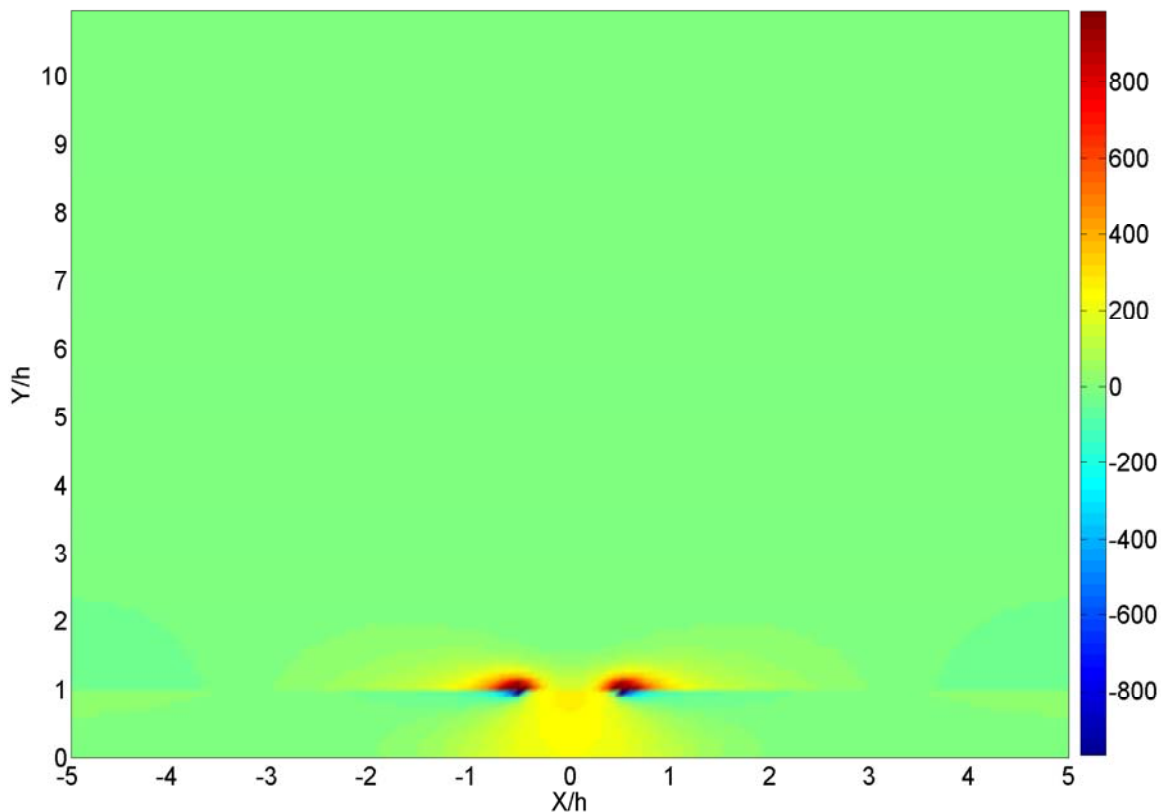
Figure 3.11 Color plot of the longitudinal Poynting vector in the corss section of microstrip line with $a = 5h, d = 10h, w = h, \varepsilon_r = \mu_r = -2.5$ at 10 GHz (actually -Pz is plotted)

3.3 Open microstrip numerical results

3.3.1 Dispersion property

If the top PEC and two side walls of the shielded microstrip are removed, then the case will be open microstrip. Here we keep all the other setup unchanged. Fig 3.12 shows the dispersion curves of open microstrip.
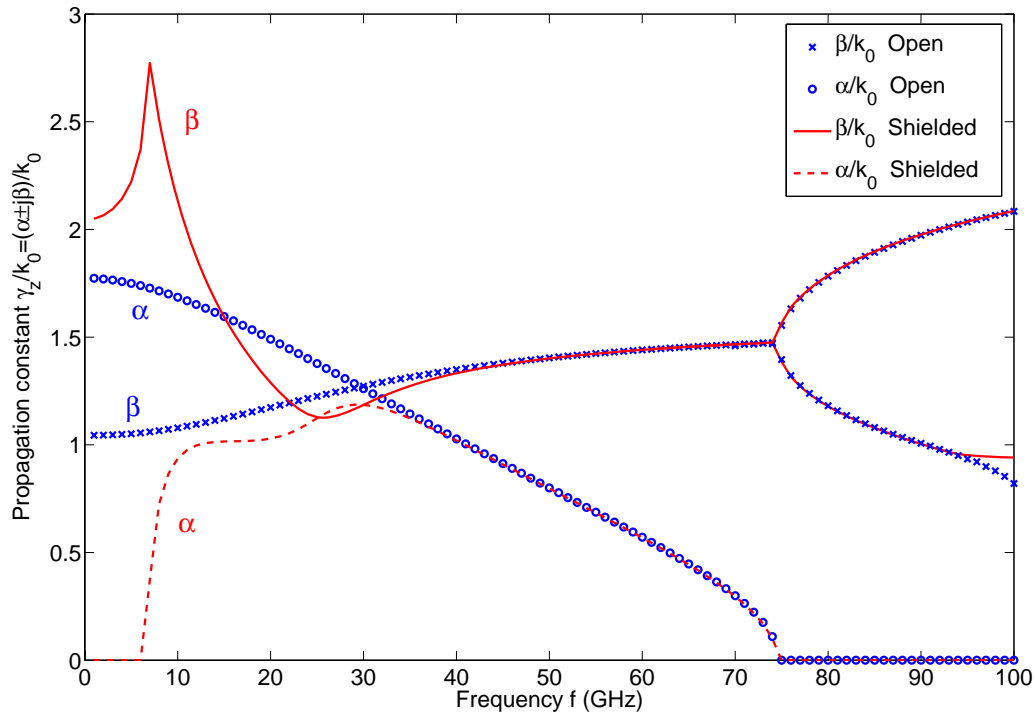
Figure 3.12 The dispersion curves of open microstrip line compared with shielded microstrip line with $\varepsilon_r = \mu_r = -2.5 \ w = h = 0.5mm$

In Fig. 3.12, the propagation constant of open microstrip line is in blue. Comparing to the shielded case, it is seen that α is non-zero below 75 GHz, which means that evanescent mode occurs. The propagation constant below 40 GHz significantly differs from the shielded microstrip line, in which propagating mode occurs at the low frequency end. As the frequency increases, the dispersion curves begin to match with the shielded case. For both open and shielded cases, we notice the two pure propagating modes above 75 GHz, except the low branch at the frequency near 100 GHz.

3.3.2 Field and power distribution

Fig. 3.13 and Fig. 3.14 show the electric and magnetic field of open microstrip line with $w = h$, $\varepsilon_r = \mu_r = -2.5$ at 5GHz. In Fig 3.13, the field vector plot is very similar to that of the shielded microstrip line with DNG metamaterials.
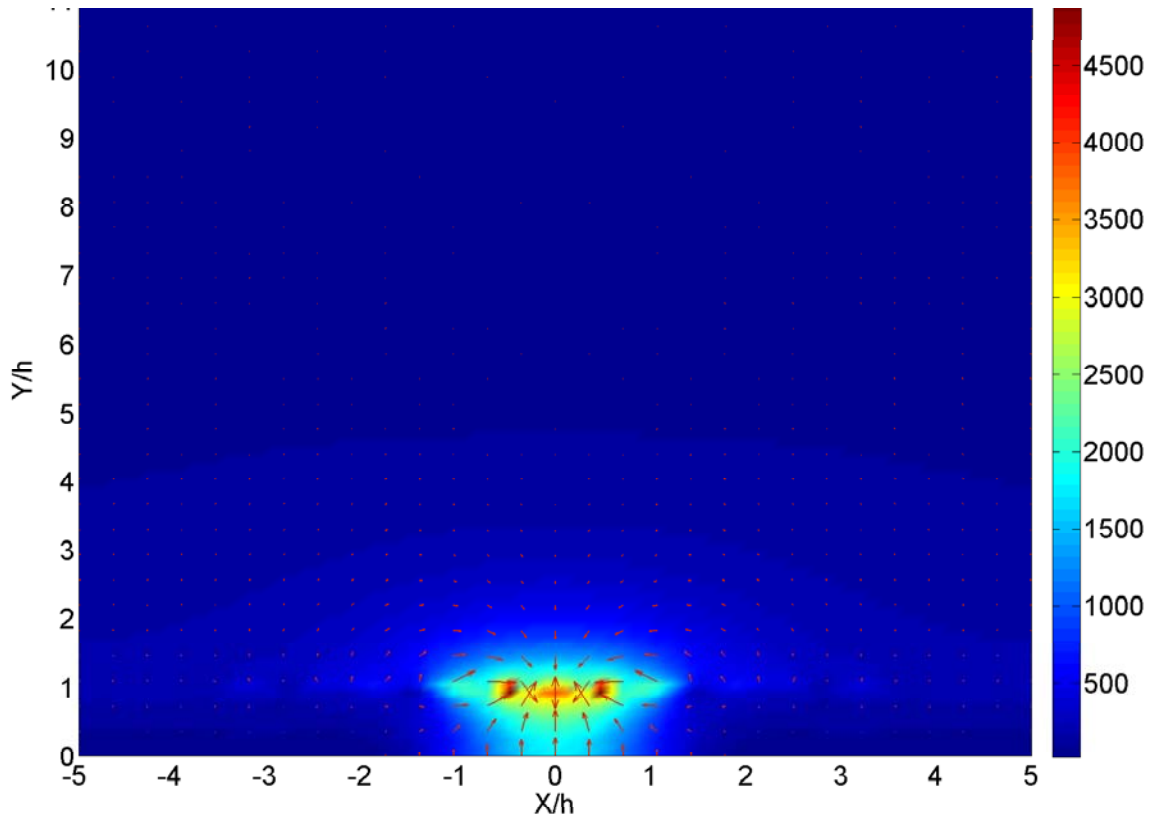
Figure 3.13 Electric field vector plot overlaid on electric field magnitude for open microstrip line with $w = h$, $\varepsilon_r = \mu_r = -2.5$ at 5 GHz
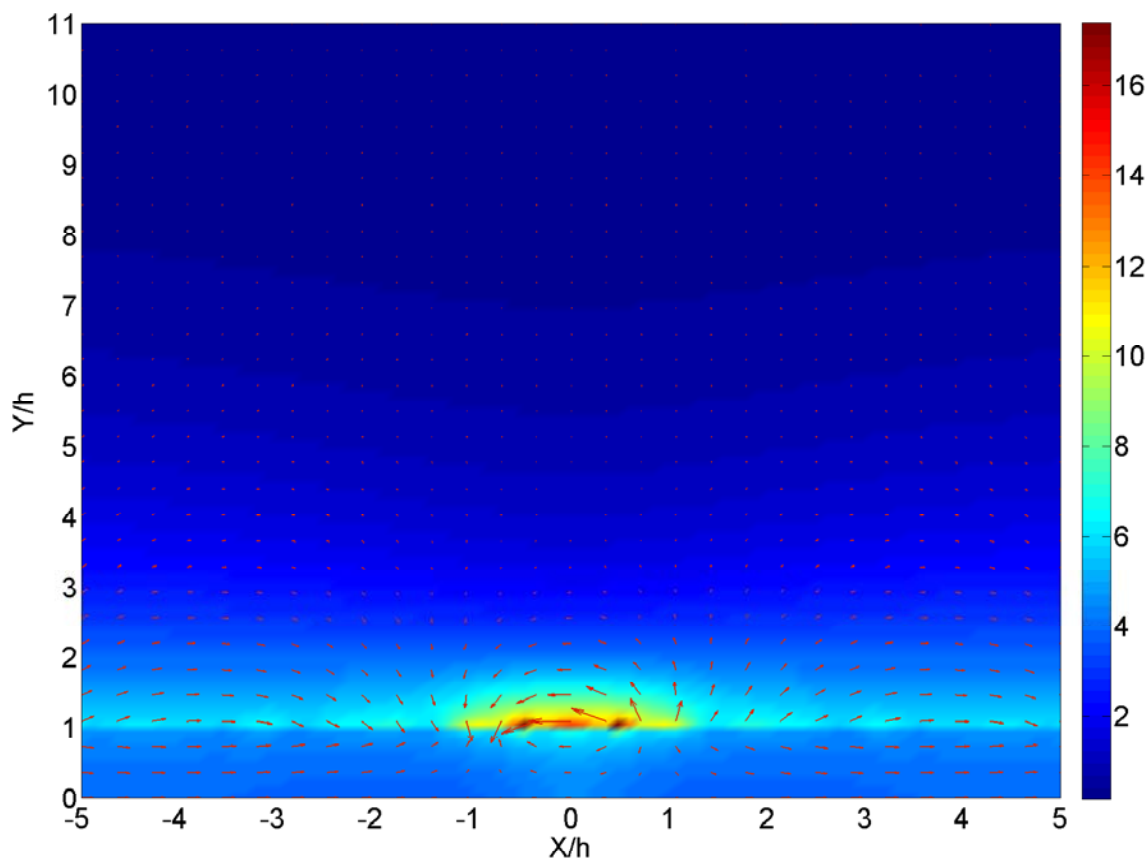
Figure 3.14 Magnetic field vector plot overlaid on magnetic field magnitude for

open microstrip line with $w = h, \varepsilon_r = \mu_r = -2.5$ at 5 GHz

Fig 3.14 shows the magnetic field distribution. Comparing with that of the shield microstrip line, we find that the region near the strip is different. In the open microstrip line, the magnetic fields in the region above and below the strip have different direction from that of region away the strip. Again, the magnetic fields in air and DNG metamaterial regions point away and towards the interface at the same time.
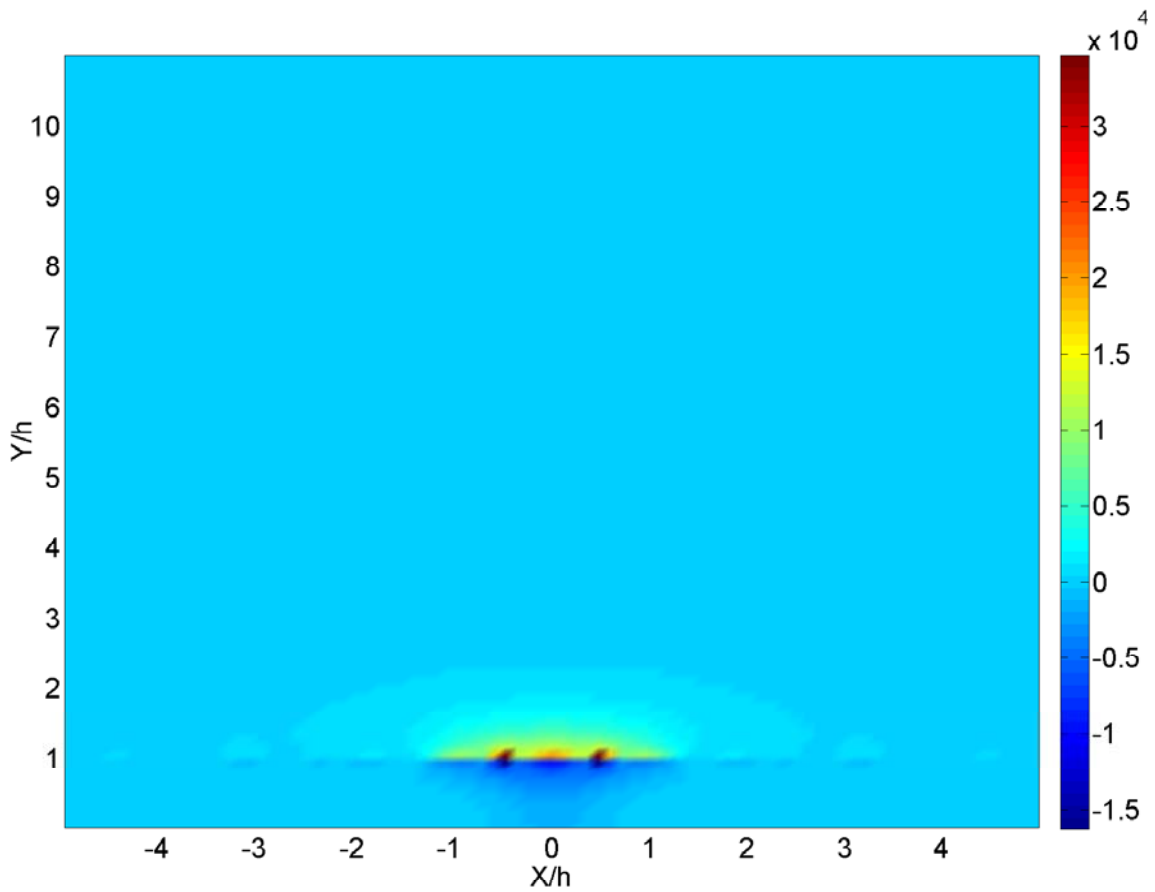
Figure 3.15 Color plot of the longitudinal Poynting vector in the corss section of

open microstrip line with $w = h, \varepsilon_r = \mu_r = -2.5$ at 5GHz (actually -Pz is plotted)

Fig 3.15 shows the color map of power distribution in open microstrip line. The power in air region has positive power and the region below the strip has negative power. The total power is zero.

3.4 Characteristic impedance

Once the total power is obtained, the characteristic impedances of microstrip lines can be estimated based on the field distribution over the whole cross section. There are three definitions for the impedance: the power-current impedance (Z_{PI}), the power-voltage impedance (Z_{PV}), and the voltage-current impedance (Z_{VI}) [23]. These three types of impedances definitions are analyzed as follows.

3.4.1 Power-current definition

In the spatial domain, the total longitude current can be calculated as the integral along x-direction.

$$I = \int_{-w/2}^{w/2} dx J_z(x) \tag{3.23}$$

With the total power in (2.71) for shielded microstrip line and (A.51) for open microstrip line, the characteristic impedance can be defined as:

$$Z_{PI} = \frac{2P}{|I_z|^2} \tag{3.24}$$

3.4.2 Power-voltage definition

The equivalent voltage on the strip can be derived as the

$$V = -\int_0^h dy E_{y1}(0, y) \tag{3.25}$$

3.4.2.1 Shielded microstrip line

In the shielded microstrip line,

$$V = -\frac{1}{2a}\int_0^h dy \sum_{m=-\infty}^{\infty} \tilde{E}_{y1}(\alpha_m, y) = -\frac{1}{2a}\sum_{m=-\infty}^{\infty}\int_0^h dy \tilde{E}_{y1}(\alpha_m, y) \quad (3.26)$$

In spectral domain, the electric field in region 1 is given as:

$$\tilde{E}_{y1} = \frac{\partial}{\partial y}\left[A\sinh(\gamma_1 y)\right] + \frac{j\alpha_m \omega \mu_1}{\beta}C\cosh(\gamma_1 y) \quad (3.27)$$

Now the integral along y direction is obtained.

$$\int_0^h dy \tilde{E}_{y1}(\alpha_m, y) = A\sinh(\gamma_1 h) + \frac{j\alpha_m \omega \mu_1}{\beta}C\frac{\sinh(\gamma_1 h)}{\gamma_1} \quad (3.28)$$

Applying the summation over α, we arrive at

$$V = -\frac{1}{2a}\sum_{m=-\infty}^{\infty}\left[A\sinh(\gamma_1 h) + \frac{j\alpha_m \omega \mu_1}{\beta}C\frac{\sinh(\gamma_1 h)}{\gamma_1}\right] \quad (3.29)$$

3.4.2.2 Open microstrip line

In the open microstrip line,

$$V = -\frac{1}{2\pi}\int_0^h dy \int_{-\infty}^{\infty} d\alpha \tilde{E}_{y1}(\alpha, y) = -\frac{1}{2\pi}\int_{-\infty}^{\infty} d\alpha \int_0^h dy \tilde{E}_{y1}(\alpha, y) \quad (3.30)$$

The integral along y direction is in the same form as that of shielded case.

$$\int_0^h dy \tilde{E}_{y1}(\alpha, y) = A\sinh(\gamma_1 h) + \frac{j\alpha \omega \mu_1}{\beta}C\frac{\sinh(\gamma_1 h)}{\gamma_1} \quad (3.31)$$

By the inverse Fourier transform, the equivalent voltage is obtained

$$V = -\frac{1}{2\pi}\int_{-\infty}^{\infty} d\alpha\left[A\sinh(\gamma_1 h) + \frac{j\alpha \omega \mu_1}{\beta}C\frac{\sinh(\gamma_1 h)}{\gamma_1}\right] \quad (3.32)$$

3.4.2.3 Power-voltage characteristic impedance

Once the total power and equivalent voltage are obtained, characteristic impedance in

the power-voltage form can be defined as:

$$Z_{PV} = \frac{|V|^2}{2P^*} \tag{3.33}$$

3.4.3 Voltage-current definition

With (3.23) and (3.25), the characteristic impedance in the voltage-current form is defined as:

$$Z_{VI} = \frac{V}{I_z} \tag{3.34}$$

CHAPTER 4. CONCLUSIONS AND FUTURE WORKS

In this thesis, the properties of DNG metamaterials have been studied. The microstrip line with DNG metamaterials below the strip and DPS above the strip is analyzed. According to different application conditions, two kinds of microstrip lines are studied, which are open and shielded.

For the shielded microstrip line, spectral domain approach is applied for the analysis. The dispersion properties can be solved by method of moments. With the obtained propagation constant, the fields in spatial domain are calculated from the spectral domain. With the fields expression, the total power can be calculated from the integral of the Poynting vector. Then Parseval's theorem is used to transfer the spatial domain to spectral domain. Dispersion curves shows that complex mode and purely propagating mode can interchangeably occur at different frequency, if the geometry of the microstrip is given. Then the microstrip geometric setup is modified to see the change of the dispersion properties. We find that the purely propagating mode will disappear, if the height of top PEC is small enough. The field distribution at arbitrary positions is plotted at different frequency.

For the open microstrip line, the dispersion curves, field distribution, power flow are analyzed similarly. Compared with the dispersion curves of shielded case, significant differences are found at the low frequency. In open microstrip, the purely propagating mode only occurs above 75 GHz. From the field plotting, the electric and magnetic field distribution is different due to the different boundary conditions.

The numerical results show that the open microsrtip line with DNG metamaterials is not a good candidate as transmission line, due to its high loss at low frequency. However, it implies that it can be used in antenna application.

One should notice that the major assumption of the above work is a non-dispersion DNG medium, while the DNG metamaterials are inherently dispersive. Thus a dispersive medium with real loss can be studied.

Furthermore, investigating a more complicated structure such as multilayer microstrip line would be more meaningful.

APPENDIX A. OPEN MICROSTRIP LINE WITH DNG METAMATERIALS

A.1. Model setup

The following figure shows the model setup for open microstrip line with DNG metamaterials.
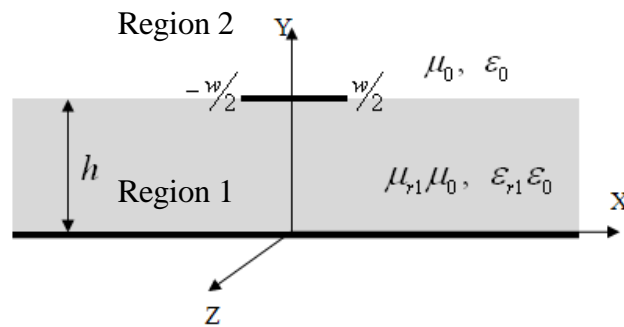
Figure A.1 Open-air microstrip line

Figure A.1 is the cross section of the open air microstrip. The bottom layer is infinite PEC. The microstrip is PEC with zero thickness. Then region 1 is filled with DNG material and region 2 is filled with air.

A.2 Spectral domain analysis

A.2.1 Vector potential

In order to obtain solutions for the electrical and magnetic fields with boundary conditions, auxiliary vector potentials are normally used. The most common vector potentials are magnetic vector potential ($\vec{A}$) and electrical vector potential ($\vec{F}$).

The vector potential of TMz mode is given as:

$$A_{zi}(x, y, z) = -\frac{\omega \mu_i \varepsilon_i}{\beta} \Phi_i^{(e)}(x, y) e^{-j\beta z} \tag{A.1}$$

The vector potential of the TEz mode is:

$$F_{zi}(x, y, z) = -\frac{\omega \mu_i \varepsilon_i}{\beta} \Phi_i^{(h)}(x, y) e^{-j\beta z} \tag{A.2}$$

The above vector potentials satisfy the Helmholtz equations at $y \neq h$:

$$\nabla_t^2 \Phi_i^{(p)}(x, y) + \left(k_i^2 - \beta^2\right) \Phi_i^{(p)}(x, y) = 0 \tag{A.3}$$

in which, $k_i^2 = \omega^2 \varepsilon_i \mu_i$, $i = 1, 2$, $p = e, h$.

With the vector potentials, we get the z-components of the electrical and magnetic

fields:

$$E_{zi} = \left[j\left(k_i^2 - \beta^2\right)/\beta \right] \Phi_i^{(e)}(x, y) e^{-j\beta z} \tag{A.4}$$

$$H_{zi} = \left[j\left(k_i^2 - \beta^2\right)/\beta \right] \Phi_i^{(h)}(x, y) e^{-j\beta z} \tag{A.5}$$

A.2.2 Fourier transform

To reduce the partial differential equations to ordinary differential equations, we apply

Fourier transform over x.

$$\tilde{f}(\alpha) = \int_{-\infty}^{\infty} dx f(x) e^{j\alpha x} \tag{A.6}$$

$$f(x) = \frac{1}{2\pi} \int_{-\infty}^{\infty} d\alpha \tilde{f}(\alpha) e^{-j\alpha x} \tag{A.7}$$

If $\tilde{f}(\alpha)$ is even function,

$$f(x) = \frac{1}{\pi} \int_{0}^{\infty} d\alpha \tilde{f}(\alpha) \cos(\alpha x) \tag{A.8}$$

If $\tilde{f}(\alpha)$ is odd function,

$$f(x) = \frac{1}{\pi} \int_0^\infty d\alpha \tilde{f}(\alpha) \sin(\alpha x) \tag{A.9}$$

For the potentials, we have

$$\tilde{\Phi}_i^{(p)}(\alpha, y) = \int_{-\infty}^\infty dx \Phi_i^{(p)}(x, y) e^{j\alpha x} \tag{A.10}$$

$$\Phi_i^{(p)}(x, y) = \frac{1}{2\pi} \int_{-\infty}^\infty d\alpha \tilde{\Phi}_i^{(p)}(\alpha, y) e^{-j\alpha x} \tag{A.11}$$

$$\int_{-\infty}^\infty dx \frac{\partial \Phi_i^{(p)}(x, y)}{\partial x} e^{j\alpha x} = (-j\alpha) \tilde{\Phi}_i^{(p)}(\alpha, y) \tag{A.12}$$

Substitute them to the Helmholtz wave equation, we get:

$$\left(\frac{d^2}{dy^2} - \gamma_i^2 \right) \tilde{\Phi}_i^{(p)}(\alpha, y) = 0 \tag{A.13}$$

in which $\gamma_i^2 = \alpha^2 + \beta^2 - k_i^2$.

Depending on the boundary conditions, the solutions to the above equation have two forms:

$$\tilde{\Phi}_i^{(p)}(\alpha, y) = A_i^{(p)}(\alpha) e^{\gamma_i y} + B_i^{(p)}(\alpha) e^{-\gamma_i y} \tag{A.14}$$

or $\qquad \tilde{\Phi}_i^{(p)}(\alpha, y) = C_i^{(p)}(\alpha) \sinh(\gamma_i y) + D_i^{(p)}(\alpha) \cosh(\gamma_i y) \tag{A.15}$

Applying the Fourier transform to the field expressions, we can get the expression in the spectral domain which is same with the shielded case.

A.2.3 Boundary conditions

With the given microstrip models, we have several boundary conditions to solve the Green functions.

Considering PEC boundary condition at $y = 0$, we have $\tilde{E}_{z1}(\alpha, 0) = 0$. Then we have

$$\tilde{\Phi}_1^{(e)}(\alpha, y) = A(\alpha)\sinh(\gamma_1 y) \tag{A.16}$$

$$\tilde{E}_{x1}(\alpha, 0) = 0 \Rightarrow \frac{\partial}{\partial y}\Phi_1^{(h)}(\alpha, y)\bigg|_{y=0} = 0 \qquad \text{we have}$$

$$\tilde{\Phi}_1^{(h)}(\alpha, y) = C(\alpha)\cosh(\gamma_1 y) \tag{A.17}$$

When y is increasing to infinite, the filed in the medium 2 should decrease to zero. So we

have:

$$\tilde{\Phi}_2^{(e)}(\alpha, y) = B(\alpha)e^{-\gamma_2(y-h)} \tag{A.18}$$

$$\tilde{\Phi}_2^{(h)}(\alpha, y) = D(\alpha)e^{-\gamma_2(y-h)} \tag{A.19}$$

In order to get the parameters ABCD, four other boundary conditions are needed. The

tangential field on the interface should be continuous. It means:

$$\begin{aligned}
\tilde{E}_{z1}(\alpha, h) &= \tilde{E}_{z2}(\alpha, h) \\
\tilde{E}_{x1}(\alpha, h) &= \tilde{E}_{x2}(\alpha, h)
\end{aligned} \tag{A.20}$$

Substitute (2.26) into (A.20), we arrive at

$$\left(k_1^2 - \beta^2\right)A\sinh(\gamma_1 h) = \left(k_2^2 - \beta^2\right)B \tag{A.21}$$

$$j\alpha\left[A\sinh(\gamma_1 h) - B\right] = \frac{\omega}{\beta}\left[\gamma_1\mu_1 C\sinh(\gamma_1 h) + \mu_2\gamma_2 D\right] \tag{A.22}$$

At $y = h$, the boundary condition for the magnetic field in spatial domain is:

$$\hat{y} \times \left(\bar{H}_2 - \bar{H}_1\right) = \bar{J}_s \tag{A.23}$$

Because the surface current is in the x- and z- directions, we can write:

$$\bar{J}_s(x, y = h, z) = \left[\hat{x}J_x(x) + \hat{z}J_z(x)\right]e^{-j\beta z} \tag{A.24}$$

Then we get the boundary condition in spectral domain:

$$\hat{y} \times \left[\tilde{\bar{H}}_2(\alpha, h) - \tilde{\bar{H}}_1(\alpha, h) \right] = \hat{x} \tilde{J}_x(\alpha) + \hat{z} \tilde{J}_z(\alpha) \tag{A.25}$$

For z-component:

$$j \frac{k_2^2 - \beta^2}{\beta} D - j \frac{k_1^2 - \beta^2}{\beta} C \cosh(\gamma_1 h) = \tilde{J}_x(\alpha) \tag{A.26}$$

For x-component:

$$-j\alpha \left[D - C\cosh(\gamma_1 h) \right] + \frac{\omega}{\beta} \left[\varepsilon_1 \gamma_1 \cosh(\gamma_1 h) + \varepsilon_2 \gamma_2 B \right] = -\tilde{J}_z(\alpha) \tag{A.27}$$

Now we have four coupled equations with four unknowns. To solve the equations, we rewrite them in matrix form:

$$\begin{pmatrix} -(k_1^2 - \beta^2)\sinh(\gamma_1 h) & (k_2^2 - \beta^2) & 0 & 0 \\ \alpha\beta\sinh(\gamma_1 h) & -\alpha\beta & j\omega\mu_1\gamma_1\sinh(\gamma_1 h) & j\omega\mu_2\gamma_2 \\ 0 & 0 & (k_1^2 - \beta^2)\cosh(\gamma_1 h) & -(k_2^2 - \beta^2) \\ j\omega\varepsilon_1\gamma_1\cosh(\gamma_1 h) & j\omega\varepsilon_2\gamma_2 & -\alpha\beta\cosh(\gamma_1 h) & \alpha\beta \end{pmatrix} \begin{pmatrix} A \\ B \\ C \\ D \end{pmatrix} = \begin{pmatrix} 0 \\ 0 \\ j\beta\tilde{J}_x \\ -j\beta\tilde{J}_z \end{pmatrix} \tag{A.28}$$

Solving the above matrix problem, we get the parameters ABCD.

$$B = -\frac{1}{\Delta}\left[F_1 b_{22} + \frac{\alpha\beta}{k_1^2 - \beta^2} b_{12} \right] \tilde{J}_x(\alpha) + \frac{1}{\Delta} b_{12} \tilde{J}_z(\alpha)$$

$$D = -\frac{1}{\Delta}\left[F_1 b_{21} + \frac{\alpha\beta}{k_1^2 - \beta^2} b_{11} \right] \tilde{J}_x(\alpha) + \frac{1}{\Delta} b_{11} \tilde{J}_z(\alpha) \tag{A.29}$$

where $\Delta = -\frac{\omega^2}{\beta^2} \frac{k_2^2 - \beta^2}{k_1^2 - \beta^2} \left[\mu_2 \gamma_1 \coth(\gamma_1 h) + \mu_1 \gamma_2 \right] \left[\varepsilon_2 \gamma_1 \tanh(\gamma_1 h) + \varepsilon_1 \gamma_2 \right]$

By the boundary condition, we can get:

$$A = \frac{k_2^2 - \beta^2}{k_1^2 - \beta^2} \frac{B}{\sinh(\gamma_1 h)}$$

$$C = \left[\frac{j\beta}{k_1^2 - \beta^2} \tilde{J}_x + \frac{k_2^2 - \beta^2}{k_1^2 - \beta^2} D \right] \bigg/ \cosh(\gamma_1 h) \tag{A.30}$$

A.2.4 Green functions

Now let's look at the field at the interface of region 1 and region 2. The spatial domain fields are given as:

$$E_{x2}(x,y) = \frac{\partial}{\partial x}\Phi_2^{(e)}(\alpha,y) + \frac{\omega\mu_2}{\beta}\frac{\partial}{\partial y}\Phi_2^{(h)}(\alpha,y)$$

$$E_{z2}(x,y) = j\frac{k_2^2 - \beta^2}{\beta}\Phi_2^{(e)}(\alpha,y) \tag{A.31}$$

The spectral domain fields:

$$\tilde{E}_{x2}(\alpha,h) = -j\alpha B(\alpha) - \frac{\omega\mu_2}{\beta}D(\alpha)$$

$$= G_{xx}(\alpha,\beta)\tilde{J}_x(\alpha) + G_{xz}(\alpha,\beta)\tilde{J}_z(\alpha) \tag{A.32}$$

$$\tilde{E}_{z2}(\alpha,h) = j\frac{k_2^2 - \beta^2}{\beta}B(\alpha)$$

$$= G_{zx}(\alpha,\beta)\tilde{J}_x(\alpha) + G_{zz}(\alpha,\beta)\tilde{J}_z(\alpha) \tag{A.33}$$

The Green's functions are:

$$G_{xx}(\alpha,\beta) = \frac{-j\eta_2}{k_2\Delta}\left[\left(k_1^2 - \alpha^2\right)\gamma_2 + \mu_r\left(k_2^2 - \alpha^2\right)\gamma_1\tanh(\gamma_1 h)\right]$$

$$G_{xz}(\alpha,\beta) = G_{zx}(n,\beta) = \frac{-j\eta_2\alpha\beta}{k_2\Delta}\left[\gamma_2 + \mu_r\gamma_1\tanh(\gamma_1 h)\right] \tag{A.34}$$

$$G_{zz}(\alpha,\beta) = \frac{-j\eta_2}{k_2\Delta}\left[\left(k_1^2 - \beta^2\right)\gamma_2 + \mu_r\left(k_2^2 - \beta^2\right)\gamma_1\tanh(\gamma_1 h)\right]$$

$$\Delta = \left[\varepsilon_r\gamma_2 + \gamma_1\tanh(\gamma_1 h)\right]\left[\mu_r\gamma_2 + \gamma_1\coth(\gamma_1 h)\right]$$

where $\varepsilon_r = \varepsilon_1/\varepsilon_2$, $\mu_r = \mu_1/\mu_2$.

A.3 Galerkin's methods

For the open air microstrip, the tangential electrical field components at the interface can be found in (A.32) and (A.33).

With Parseval's theorem, multiplying basis on both sides of (A.32) and (A.33) as in the shielded case, then we arrive at

$$
\begin{aligned}
& \int_{-\infty}^{\infty} \tilde{J}_{xm}(\alpha) \tilde{E}_{x2}(\alpha, h) d\alpha \\
& = \int_{-\infty}^{\infty} d\alpha \left[G_{xx}(\alpha, \beta) \tilde{J}_{x}(\alpha) + G_{xz}(\alpha, \beta) \tilde{J}_{z}(\alpha) \right] \tilde{J}_{xm}(\alpha) \\
& = 2\pi \int_{-\infty}^{\infty} dx J_{xm}(x) E_{x2}(-x, h)
\end{aligned}
\tag{A.35}
$$

$$
\begin{aligned}
& \int_{-\infty}^{\infty} \tilde{J}_{zm}(\alpha) \tilde{E}_{z2}(\alpha, h) d\alpha \\
& = \int_{-\infty}^{\infty} d\alpha \left[G_{zx}(\alpha, \beta) \tilde{J}_{xm}(\alpha) + G_{zz}(\alpha, \beta) \tilde{J}_{zm}(\alpha) \right] \tilde{J}_{zm}(\alpha) \\
& = 2\pi \int_{-\infty}^{\infty} dx J_{zm}(x) \tilde{E}_{z2}(-x, h)
\end{aligned}
\tag{A.36}
$$

With the above equations, we can fill the elements into the matrix

$$
\begin{pmatrix} K_{xx} & K_{xz} \\ K_{zx} & K_{zz} \end{pmatrix} \begin{pmatrix} A \\ B \end{pmatrix} = 0
\tag{A.37}
$$

Referring to (2.56), the elements of K matrix are obtained.

$$
\begin{aligned}
K_{xx}^{mn} &= \int_{-\infty}^{\infty} \tilde{J}_{xm}(\alpha) G_{xx}(\alpha, \beta) \tilde{J}_{xn}(\alpha) d\alpha \\
K_{xz}^{mn} &= K_{zx}^{mn} = \int_{-\infty}^{\infty} \tilde{J}_{xm}(\alpha) G_{xz}(\alpha, \beta) \tilde{J}_{zn}(\alpha) d\alpha \\
K_{zz}^{mn} &= \int_{-\infty}^{\infty} \tilde{J}_{zm}(\alpha) G_{zz}(\alpha, \beta) \tilde{J}_{zn}(\alpha) d\alpha
\end{aligned}
\tag{A.38}
$$

A.4 Field distributions

In the above parts, we get the potential expressions in the spectral domain:

$$
\begin{aligned}
\tilde{\Phi}_1^{(e)}(\alpha, y) &= A(\alpha) \sinh(\gamma_1 y) \\
\tilde{\Phi}_1^{(h)}(\alpha, y) &= C(\alpha) \cosh(\gamma_1 y) \\
\tilde{\Phi}_2^{(e)}(\alpha, y) &= B(\alpha) e^{-\gamma_2(y-h)} \\
\tilde{\Phi}_2^{(h)}(\alpha, y) &= D(\alpha) e^{-\gamma_2(y-h)}
\end{aligned}
\tag{A.39}
$$

where $\Phi_i^{(e)}(x, y)$ is an even function of x, and $\Phi_i^{(h)}(x, y)$ is an odd function of x.

Region 1

$$\Phi_1^{(e)}(x,y) = \frac{1}{\pi}\int_0^\infty A(\alpha)\sinh(\gamma_1 y)\cos(\alpha x)d\alpha$$

$$\Phi_1^{(h)}(x,y) = \frac{-j}{\pi}\int_0^\infty C(\alpha)\cosh(\gamma_1 y)\sin(\alpha x)d\alpha$$

$$\frac{\partial}{\partial x}\Phi_1^{(e)}(x,y) = \frac{-1}{\pi}\int_0^\infty A(\alpha)\sinh(\gamma_1 y)\alpha\sin(\alpha x)d\alpha \qquad (A.40)$$

$$\frac{\partial}{\partial x}\Phi_1^{(h)}(x,y) = \frac{-j}{\pi}\int_0^\infty C(\alpha)\cosh(\gamma_1 y)\alpha\cos(\alpha x)d\alpha$$

$$\frac{\partial}{\partial y}\Phi_1^{(e)}(x,y) = \frac{1}{\pi}\int_0^\infty A(\alpha)\gamma_1\cosh(\gamma_1 y)\cos(\alpha x)d\alpha$$

$$\frac{\partial}{\partial y}\Phi_1^{(h)}(x,y) = \frac{-j}{\pi}\int_0^\infty C(\alpha)\gamma_1\sinh(\gamma_1 y)\sin(\alpha x)d\alpha$$

Region 2

$$\Phi_2^{(e)}(x,y) = \frac{1}{\pi}\int_0^\infty d\alpha B(\alpha)e^{-\gamma_2(y-h)}\cos(\alpha_n x)$$

$$\Phi_2^{(h)}(x,y) = \frac{-j}{\pi}\int_0^\infty d\alpha D(\alpha)e^{-\gamma_2(y-h)}\sin(\alpha_n x)$$

$$\frac{\partial}{\partial x}\Phi_2^{(e)}(x,y) = \frac{-1}{\pi}\int_0^\infty d\alpha B(\alpha)e^{-\gamma_2(y-h)}\alpha\sin(\alpha x) \qquad (A.41)$$

$$\frac{\partial}{\partial x}\Phi_2^{(h)}(x,y) = \frac{-j}{\pi}\int_0^\infty d\alpha D(\alpha)e^{-\gamma_2(y-h)}\alpha\cos(\alpha x)$$

$$\frac{\partial}{\partial y}\Phi_2^{(e)}(x,y) = \frac{-1}{\pi}\int_0^\infty d\alpha B(\alpha)\gamma_2 e^{-\gamma_2(y-h)}\cos(\alpha x)$$

$$\frac{\partial}{\partial y}\Phi_2^{(h)}(x,y) = \frac{j}{\pi}\int_0^\infty d\alpha D(\alpha)\gamma_2 e^{-\gamma_2(y-h)}\sin(\alpha x)$$

Substituting the above spatial domain expressions into spatial field expressions, we get

the field distribution in spatial domain.

A.5 Power flow

For the open microstrip, the top PEC layer and two side walls are removed. So the

integral range over y-direction is from zero to infinity. Moreover, along x-direction, integral

should be used. So the Parseval's theorem must be modified to the integral form. The

expression for total power is given as:

$$P = \frac{1}{2}\int_0^\infty \int_{-\infty}^\infty \vec{E} \times \vec{H}^* \cdot \hat{z}\, dx\, dy = \frac{1}{4\pi}\int_{-\infty}^\infty \int_0^\infty \left(\tilde{E}_{x,i}\tilde{H}_{y,i}^* - \tilde{E}_{y,i}\tilde{H}_{y,i}^* \right) dy\, d\alpha \tag{A.42}$$

Similarly, to fulfill the integral in the spectral domain, the field expressions are listed.

$$\tilde{E}_{x1}(\alpha, y) = \left(-j\alpha A + \frac{\omega\mu_1\gamma_1 C}{\beta} \right)\sinh(\gamma_1 y)$$

$$\tilde{E}_{x2}(\alpha, y) = \left(-j\alpha B - \frac{\omega\mu_2\gamma_2}{\beta} D \right)e^{-\gamma_2(y-h)}$$

$$\tilde{E}_{y1}(\alpha, y) = \left(A\gamma_1 + \frac{j\alpha\omega\mu_1}{\beta} C \right)\cosh(\gamma_1 y) \tag{A.43}$$

$$\tilde{E}_{y2}(\alpha, y) = \left(-B\gamma_2 + \frac{j\alpha\omega\mu_2}{\beta} D \right)e^{-\gamma_2(y-h)}$$

$$\tilde{H}_{x1}(\alpha, y) = \left(-j\alpha C - \frac{\omega\varepsilon_1\gamma_1}{\beta} A \right)\cosh(\gamma_1 y)$$

$$\tilde{H}_{x2}(\alpha, y) = \left(-j\alpha D + \frac{\omega\varepsilon_2\gamma_2 B}{\beta} \right)e^{-\gamma_2(y-h)}$$

$$\tilde{H}_{y1}(\alpha, y) = \left(C\gamma_1 - \frac{j\alpha\omega\varepsilon_1 A}{\beta} \right)\sinh(\gamma_1 y) \tag{A.44}$$

$$\tilde{H}_{y2}(\alpha, y) = \left(-D\gamma_2 - \frac{j\alpha\omega\varepsilon_2 B}{\beta} \right)e^{-\gamma_2(y-h)}$$

Multiplying electrical field and magnetic field,

Region 1:

$$\tilde{E}_{x1}(\alpha, y)\tilde{H}_{y1}^*(\alpha, y) = K_A \sinh(\gamma_1 y)\sinh(\gamma_1^* y)$$

$$\tilde{E}_{y1}(\alpha, y)\tilde{H}_{x1}^*(\alpha, y) = K_B \cosh(\gamma_1 y)\cosh(\gamma_1^* y) \tag{A.45}$$

where

$$K_A = \left(-j\alpha A + \frac{\omega\mu_1\gamma_1 C}{\beta} \right)\left(C\gamma_1 + \frac{j\alpha\omega\varepsilon_1 A}{\beta} \right)^*$$

$$K_B = \left(A\gamma_1 + \frac{j\alpha\omega\mu_1}{\beta} C \right)\left(-j\alpha C - \frac{\omega\varepsilon_1\gamma_1}{\beta} A \right)^*$$

Region 2:

$$\tilde{E}_{x2}(\alpha, y)\tilde{H}_{y2}^*(\alpha, y) = K_C e^{-\gamma_2(y-h)}e^{-\gamma_2^*(y-h)}$$

$$\tilde{E}_{y2}(\alpha, y)\tilde{H}_{x2}^*(\alpha, y) = K_D e^{-\gamma_2(y-h)}e^{-\gamma_2^*(y-h)}$$

(A.46)

where

$$K_C = \left(-j\alpha B - \frac{\omega\mu_2\gamma_2}{\beta}D\right)\left(-D\gamma_2 - \frac{j\alpha\omega\varepsilon_2 B}{\beta}\right)^*$$

$$K_D = \left(-B\gamma_2 + \frac{j\alpha\omega\mu_2}{\beta}D\right)\left(-j\alpha D + \frac{\omega\varepsilon_2\gamma_2 B}{\beta}\right)^*$$

Then we come to:

$$\tilde{E}_{x1}(\alpha, y)\tilde{H}_{y1}^*(\alpha, y) - \tilde{E}_{y1}(\alpha, y)\tilde{H}_{x1}^*(\alpha, y)$$

$$= K_A \sinh(\gamma_1 y)\sinh(\gamma_1^* y) - K_B \cosh(\gamma_1 y)\cosh(\gamma_1^* y)$$

$$= \frac{1}{4}\left[(K_A - K_B)\left(e^{2R_1 y} + e^{-2R_1 y}\right) - (K_A + K_B)\left(e^{2jI_1 y} + e^{-2jI_1 y}\right)\right]$$

(A.47)

$$\tilde{E}_{x2}(\alpha, y)\tilde{H}_{y2}^*(\alpha, y) - \tilde{E}_{y2}(\alpha, y)\tilde{H}_{x2}^*(\alpha, y)$$

$$= K_C e^{-\gamma_2(y-h)}e^{-\gamma_2^*(y-h)} - K_D e^{-\gamma_2(y-h)}e^{-\gamma_2^*(y-h)}$$

$$= (K_C - K_D)e^{-2R_2(y-h)}$$

(A.48)

The integral over y-direction is derived in the close form separately for both regions.

$$P_1(\alpha) = \int_0^h dy\left[\tilde{E}_{x1}(\alpha, y)\tilde{H}_{y1}^*(\alpha, y) - \tilde{E}_{y1}(\alpha, y)\tilde{H}_{x1}^*(\alpha, y)\right]$$

$$= \frac{1}{4}\left[(K_A - K_B)\left(\frac{e^{2R_1 h} - e^{-2R_1 h}}{2R_1}\right) - (K_A + K_B)\left(\frac{e^{2jI_1 h} - e^{-2jI_1 h}}{2I_1 j}\right)\right]$$

(A.49)

$$P_2(\alpha) = \int_h^\infty dy\left[\tilde{E}_{x2}(\alpha, y)\tilde{H}_{y2}^*(\alpha, y) - \tilde{E}_{y2}(\alpha, y)\tilde{H}_{x2}^*(\alpha, y)\right]$$

$$= (K_C - K_D)\frac{1}{2R_2}$$

(A.50)

Finally, the total power can be calculated through the integral over α.

$$P = \frac{1}{2}\int_0^\infty \int_{-\infty}^\infty \bar{E} \times \bar{H}^* \cdot \hat{z}\,dxdy = \frac{1}{2\pi}\int_0^\infty \left[P_1(\alpha) + P_2(\alpha)\right]d\alpha$$

(A.51)

BIBLIOGRAPHY

[1] V. G. Veselago, "Electrodynamics of substances with simultaneously negative values of ε and μ," *Soviet Physics USPEKI*, vol. 10, pp. 509–514, 1968.

[2] J. B. Pendry, "Negative refraction makes a perfect lens," *Phys. Rev. Lett.,* vol. 85, pp. 3966–3969, October 2000.

[3] N. Engheta and R. W. Ziolkowski, "A Positive Future for Double-Negative Metamaterials," *IEEE Trans. Microwave Theory Tech.,* vol. 53, pp. 1535- 1556, April 2005.

[4] J. B. Pendry, A. J. Holden, D. J. Robbins, and W. J. Stewart, "Magnetism from conductors and enhanced nonlinear phenomena," *IEEE Trans. Microwave Theory Tech.,* vol. 47, pp.2075–2084, November 1999.

[5] J. B. Pendry, A. J. Holden, W. J. Stewart, and I. Youngs, "Extremely low frequency plasmons in metallic mesostructures," *Phys. Rev. Lett.,* vol. 76, pp. 4773–4776, June 1996.

[6] D. R. Smith, W. J. Padilla, D. C. Vier, S. C. Nemat-Nasser, and S. Schultz, "Composite medium with simultaneously negative permeability and permittivity," *Phys. Rev. Lett.*, vol. 84, pp. 4184–4187, May 2000.

[7] D. R. Smith and N. Kroll, "Negative refractive index in left-handed materials," *Phys. Rev. Lett.*, vol. 85, pp. 2933–2936, October 2000.

[8] R. A. Shelby, D. R. Smith, and S. Schultz, "Experimental verification of a negative index of refraction," *Science*, vol. 292, pp. 72–79, April 2001.

[9] T. Itoh and R. Mittra, "Spectral domain approach for calculating the dispersion characteristics of microstrip lines," *IEEE Trans. Microwave Theory Tech.*, vol. 21, pp. 496-499, July 1973.

[10] ——, "A new technique for analysis of dispersion characteristics of microstrip lines," *IEEE Trans. Microwave Theory Tech.*, vol. 19, pp.47-56, January 1971.

[11] ——, "A technique for computing dispersion characteristics of shielded microstrip lines," *IEEE Trans. Microwave Theory Tech.*,vol. 22, pp.896-898. October 1974.

[12] C. A. Balanis, *Advanced Engineering Electromagnetics*, John Wiley Sons, Inc., 1989.

[13] R. E. Collin, *Field Theory of Guided Waves*, New York: IEEE Press, 2nd ed., 1991, p. 304.

[14] M. Kobayashi and H. Sekine, "Closed-form expressions for the current distributions on open microstrip lines," *IEEE Trans. Microwave Theory Tech.*, vol. 39, pp. 1115-1119, July 1991.

[15] L. Zhang, "Accurate electromagnetic full-wave modeling for interconnects in semiconductor integrated circuits," *Ph.D Thesis*, Iowa State University, Ames, Iowa, 2007.

[16] W. Shu and J.M. Song, "Complete mode spectrum of a grounded dielectric slab with double negative metamaterials," *Progress in Electromagnetics Research,* PIER 65, J.A. Kong (ed.), pp. 103-123, EMW Publishing, Cambridge, MA 2006.

[17] W. Shu, "Electromagnetic waves in double negative metamaterials and study on numerical resonances in the method of moments (MoM)," *Ph.D Thesis*, Iowa State University, Ames, Iowa, 2008.

[18]   S. Moriguchi, K. Udagawa, and S. Ichimatsu, *Mathematical Formulae III*, Tokoyo: Iwanami Co., 1977, pp. 193-197.

[19]   H. Bateman, *Tables of Integral Transforms, Volume I,* New York, McGraw-Hill Book Company, Inc., 1954.

[20]   K. Uchida, T. Noda, and T. Matsunaga, "New type of spectral-domain analysis of a microstrip line," *IEEE Trans. Microwave Theory Tech.*, vol. 37, pp. 947-952, June 1989.

[21]   C. M. Krowne, "Physics of Propagation in left-handed guided wave structures at microwave and millimeter-wave frequencies," *Phys. Rev. Lett.,* vol 92, pp. 53901 53904, February 2004.

[22]   ——, "Electromagnetic-field theory and numerically generated results for propagation in left-handed guided-wave single-microstrip structures," *IEEE Trans. Microwave Theory Tech.*, vol. 51, no. 12, pp. 2269–2283, December 2003.

[23]   G. Cano, F. Medina, and M. Horno, "Efficient spectral domain analysis of generalized multistrip lines in stratified media including thin, anisotropic and lossy substrates," *IEEE Trans. Microwave Theory Tech*, vol. 40, no. 2, pp. 217-227, February 1992.